Diagnostic study of geomagnetic storm-induced ionospheric changes over VLF signal propagation paths in mid-latitude D-region

Victor U. J. Nwankwo[1], William Denig[2], Sandip K. Chakrabarti[3], Olugbenga Ogunmodimu[4], Muyiwa P. Ajakaiye[1], Johnson O. Fatokun[1], Paul I. Anekwe[1], Omodara E. Obisesan[1], Olufemi E. Oyanameh[1], and Oluwaseun V. Fatoye[1]

[1]Space, Atmospheric Physics and Radio waves Propagation Laboratory, Anchor University, Lagos, Nigeria
[2]St. Joseph College of Maine, Standish, ME 04084, U.S.A
[3]Indian Centre for Space Physics, Kolkata-700084, India
[4]Department of Electrical Engineering, Manchester Metropolitan University, Manchester, UK

Correspondence: Victor U. J. Nwankwo (vnwankwo@aul.edu.ng)

Abstract. We performed a diagnostic study of geomagnetic storm-induced disturbances that are coupled to the mid-latitude D-region by quantifying the propagation characteristics of very low frequency (VLF) radio signals from transmitters located in Cumbria, U.K. (call sign GQD) and Rhauderfehn, Germany (DHO) and received in southern France (A118). We characterised the diurnal VLF amplitudes from two propagation paths into five metrics, namely the mean amplitude before sunrise (MBSR), the midday amplitude peak (MDP), the mean amplitude after sunset (MASS), the sunrise terminator (SRT) and the sunset terminator (SST). We analyzed and monitored trends in the variation of signal metrics for up to 20 storms, to attribute the deviations in the signal amplitudes that were attributable to the storms. Five storms and their effects on the signals were examined in further detail. Our results indicate that relative to pre-storm levels the storm-day MDP exhibited characteristic decreases in about 80% (67%) of the events for the DHO-A118 (GQD-A118) propagation paths, respectively. The MBSR showed decreases of about 60% (77%) whereas the MASS decreased by 67% (58%). Conversely, the SRT and SST showed amplitude decreases of 33% (25%) and 47% (42%), respectively. Of the two propagation paths used in this study, the amplitude decreases for the DHO-A118 propagation path signal was greater as previously noted by Nwankwo et al. 2016. To better understand the state of the ionosphere over the signal propagation paths and how it might have affected the VLF amplitudes we further analyzed the virtual heights (h'E, h'F1 and h'F2) and critical frequencies (foE, foF1, and foF2) from ionosondes located near the transmitter locations. The results of this analysis showed significant increases and fluctuations in both the F-region critical frequencies and virtual heights above the transmitters during the geomagnetic storms. The largest increases in the virtual heights occurred near the DHO transmitter in Germany suggesting a strong storm response over the region which might account for the larger MDP decrease along the DHO-A118 propagation path.

1 Introduction

The terrestrial magnetosphere is formed by the interaction between the solar wind and the earth's magnetic field (McPherron et al., 2008). In contrast, the ionosphere is largely the result of solar photoionization of the neutral atmosphere balanced against chemical recombination and particle transport (Prolss, 2004; Kelley, 2009). The magnetosphere and ionosphere are coupled via the geomagnetic field effectively tying these seemingly disparate regions into a global magnetosphere-ionosphere (M-I) system (Blanc, 1988; Nwankwo et al., 2016). Within the concept of an open magnetosphere (Dungey, 1961) energy is transferred from the solar wind to the M-I system via magnetic reconnection (Cassak, 2016). Variations within the interplanetary environment, driven by solar disturbances, affect the M-I system particularly when the interplanetary magnetic field (IMF), embedded within the solar wind, is oriented southward relative to the outer northward-directed geomagnetic field (Gonzalez et al., 1999; Liu and Li, 2002). A geomagnetic storm is triggered when the solar-terrestrial interaction is sufficiently intense to energize the ring current (Jordanova et al., 2020) and to solicit a negative response in ground-based magnetometers in terms of the Disturbance storm time (Dst) index (Russel et al., 1974; Mayaud, 1980; Borovsky and Shprits, 2017). The strength of a geomagnetic storm is typically classified as small, moderate or intense for Dst values less than (<) -30 nT, < -50 nT, and < -100 nT, respectively (Gonzalez et al., 1994). The two leading drivers of geomagnetic storms are coronal mass ejections (CMEs) and corotating interactive regions (CIRs) (Baker, 2000). A CME is the impulsive release of solar material into interplanetary space from a solar active region that may, or may not, be associated with a solar flare (Youssef, 2012). Conversely, a CIR is the result of a high-speed stream (HSS) emitted from a solar coronal hole overtaking the background solar wind (Choi et al., 2009). In both cases the shock front at the leading edge of the interplanetary disturbance increases the ram pressure imposed on the dayside magnetopause causing a reconfiguration of the dayside Chapman-Ferraro current system (Chapman and Ferraro, 1930) and, in turn, the magnetosphere as a whole (Ganushkina et al., 2018). A typical geomagnetic storm has three phases consisting of 1) a sudden storm commencement (SSC) at the time of the increased ram pressure, 2) a main phase as the ring current is energized and 3) a recovery phase as the magnetosphere returns to a more quiescent ground state (Akasofu, 2018; Gonzalez et al., 1994). There are distinct differences between how and when CME-driven versus CIR-driven storms affect the earth (Borovsky and Denton, 2006). Typically, CME-driven storms are stronger, with regards to Dst (Tsurutani et al., 2006) and occur more frequently near the maximum in the sun's 11-year activity cycle (Gonzalez et al., 1999) whereas CIR-driven storms are weaker and occur predominantly on the decreasing phase of solar activity (Tsurutani et al., 1995). While the impacts of both CME and CIR-driven geomagnetic storms on the middle-to-upper atmosphere have been extensively studied and well known (Fuller-Rowell et al., 1994; Burch, 2016; Heelis and Maute, 2020), less certain are the geomagnetic storm effects in the lower ionosphere (Lastovicka, 1996; Kumar and Kumar, 2014). For the purposes of this report our attention is limited to CME-driven, moderate geomagnetic storms and the resulting impacts on D-region Very Low Frequency (VLF) radio-wave propagation within the earth-ionosphere wave guide (EIWG). The VLF frequency band spans the range from 3 kiloHertz (kHz) to 30 kHz.

The discovery of the ionosphere is generally attributed to Carl Gauss who, in 1839, speculated on the existence of an ionized atmospheric layer to explain variations in the measured geomagnetic field (Gauss, 1938; Glassmeier and Tsurutani, 2014). Heavidside (1902) and Kennelly (1902) both independently speculated on the existence of an electrically reflecting layer following Guglielmo Marconi's demonstration (Marconi, 1901) of long-range radiowave transmission. Appleton and Barnett (1925a, b) were the first to prove the existence of this "electrical layer", or simply the E-layer, which they determined was located approximately 80 to 90 kilometers (km) above the earth's surface. The E-layer corresponded to a local maximum in the vertical electron density profile which was effective at reflecting radiowaves of up to several megahertz (Beynon, 1969). Measurements of reflecting layers both above (Appleton, 1927) and below (Colwell and Friend, 1936) the E-layer, or more generally the E-region, soon followed which were non-coincidently named the F-region and D-region, respectively. Further studies soon found a separation in the F-region that were then categorized as the F1 and F2 regions (Appleton and Naismith, 1935). These layers are the primary regions which comprise the "ionosphere", a term that was first coined by Robert Watson-Watt in 1926 and broadly adopted into the scientific lexicon after 1929 (Gardiner, 1969; Appleton, 1933). It has been long recognized that the ionosphere has both deleterious and enabling effects on terrestrial radio-wave communications, dependent on the transmission frequency band in use (Poole, 1999; Bennington, 1944). The D-region is uniquely relevant to VLF communication as a means of communication with submarines and related underwater vehicles (Moore , 1967; Waheed and Yousufzai , 2011; Lanzagorta, 2012; Sun et al., 2021).

The nominal altitudes for the D (daytime), E, F1 and F2-region peaks are 60 km, 110 km, 170 km and 300 km, respectively, although there is considerable variability within each layer depending on the solar-geophysical conditions (Mangla and Yadov, 2011). The various ionospheric layers are the result of ionization production and loss. Oliver Lodge (1902) was the first to suggest that photoionization of the background neutral atmosphere by solar ultraviolet (UV) radiation was responsible for establishing Marconi's electrically reflecting layer. Chapman (1931) codified this primary production source for the E and F layers. Solar UV radiation cannot effectively penetrate to altitudes below about 100 km (Marr , 1965). An exception is Lyman-α radiation at a wavelength of 121.5 nm within the atmospheric window of low absorption (Machol et al., 2019) and is largely responsible for maintaining the quiescent dayside D-region (Nicolet and Aikin, 1960). The complex chemical processes maintaining the ionospheric layers were initially discussed by Bates and Massey (1946, 1947) and more recently by numerous authors (Rishbeth, 1973; Schunk and Nagy, 2009; Pavlov, 2012). Ionospheric loss processes are mostly recombination, charge exchange and diffusion (Banks and Kockarts, 1973). Above about 150 km the dominant ion species is atomic oxygen whereas molecular ions are more abundant at the lower altitudes (Johnson, 1966). Consequently, dissociative recombination is the dominant loss process for the D and E-regions whereas radiative recombination and charge exchange (followed by dissociative recombination) are more prevalent closer to the F2 peak (Mangla and Yadov, 2011). Within the topside ionosphere, diffusion becomes the dominant loss process (Rishbeth, 1973). Solar flares emit photons across the electromagnetic spectrum producing a transient ionization source affecting the delicate balance of ionospheric production and loss (Mitra, 1974). X-rays, as well as gamma rays, emitted by solar flares are sufficiently energetic to penetrate the lower ionosphere and briefly dominate the ionization production rate of the dayside D-region (Hayes et al., 2021). At night the D-region electron density is greatly diminished

due to the loss of solar radiant photons whilst diffusive recombination continues unabated such that the D-region seamlessly coalesces into the lower E-region at about 90 km in the absence of other significant ionization sources (Thomas et al., 2007; Thomson and McRae, 2009). Prior to the space age, the detection of sudden ionospheric disturbances (SIDs) in the amplitude and phase of VLF radio-wave transmissions within the D-region was used as an established proxy technique for monitoring the occurrence of solar flares (Lincoln, 1964; Moral et al., 2013; Hegde et al., 2018) which were known to have a deleterious impact on radio-wave communications (Sauer and Wilkinson, 2008; Dellinger, 1937). The widely accepted standard for specifying the ionospheric electron density profile (EDP) is the empirically based International Reference Ionosphere (IRI) model which has evolved over time (Rawer et al., 1978; Rawer, 1981; Bilitza, 1990, 2001; Bilitza and Reinisch, 2008; Bilitza, 2018) with special consideration given to the D-region of the lower ionosphere (Bilitza, 1981; Friedrich and Torkar, 1992; Danilov and Smirnova, 1995; Bilitza, 1998). An alternative approach for specifying the D-region is the use of specialized atmospheric models, such as the Whole Atmosphere Community Climate Model with D-region ion chemistry (WACCM-D), which are focused on the neutral atmosphere (Verronen et al., 2016; Andersson et al., 2016; Siskind et al., 2017) which, of course, is coupled to the ionized atmosphere via chemistry (Turunen et al., 1996; Schunk, 1996, 1999; Verronen et al., 2005; Turunen et al., 2009; Kovacs et al., 2016; Verronen et al., 2016; Turunen et al., 2016; Miyoshi et al., 2021) within the overall M-I system.

Techniques used to probe the ionosphere include both ground-based and space-based approaches. The earliest methods used by Appleton and Barnett (1925b, 1926) in short-range transmitter-to-receiver trials differentiated the reflected skywave from the direct groundwave to determine the height of the E-layer. About the same time, Merve Tuve and Gregory Breit (Tuve and Breit, 1925; Breit and Tuve, 1925) proposed a methodology of using pulsed radio-wave transmissions for measuring the heights of overhead reflecting layers. The Tuve-Breit methodology was the basis for ionosondes which for many years was the preeminent scientific technique for "sounding" the ionosphere (Bibl, 1998). Ionosondes typically operate in the high frequency (HF) domain from 3 to 30 MHz to derive the vertical ionization profiles of the E and F regions. Ionosondes are quite affordable leading to their widespread use in ionospheric characterization (Stamper et al., 2005). However, a key limitation is that ground-based ionosondes can effectively measure only the "bottom-side" ionosphere at and below the F-region peaks (Reinisch and Xueqin, 1983). A variant is the space-based "topside sounder" approach from which measurements of the topside ionosphere, above the F2 peak, can be obtained (Chapman and Warren, 1968; Benson, 2010). Ionospheric profiles of the E and F regions can also be obtained using incoherent scatter radars (ISR) (Robinson et al., 2009) which are typically operated at several hundred-megahertz (MHz) within the ultra-high frequency (UHF) range (Häggström, 2017) relying on the principle of Thomson electron scattering (Farley et al., 1961; Dougherty and Farley, 1961, 1963). Conversely, coherent scatter HF radars (Greenwald et al., 1995) rely on Bragg scattering (Takefu, 1989) from ionospheric structures to probe the ionosphere (Häggström, 2017). Examples of these advanced ionospheric measuring technologies include the Alouette topside sounder (Jackson, 1986), the Millstone Hill ISR (Evans, 1969a, b) and the Super Dual Auroral (HF) Radar Network (SuperDARN) (Greenwald , 2021). More recently, researchers have leveraged the outstanding capabilities of Global Navigation Satellite Systems (GNSS), initially the Global Positioning System (GPS), for ionospheric characterization (Davies and Hartmann, 1997) using receivers on the ground (Mannucci et al., 1998; Prol et al., 2021) and in space (Mannucci et al., 2020). The Continuously

Operating Reference Stations (CORS) (Snay and Soler, 2008) is a good example of a ground-based GNSS network whereas the Constellation Observing System for Meteorology, Ionosphere, and Climate (COSMIC) (Yue et al, 2014) is an example of the related space-based approach. With regard to the lower E and D region, none of the aforementioned technologies are particularly effective at monitoring the bottommost ionospheric region (Cummer et al., 1998; Kumar et al., 2015) which is the focus of the present work. However, the perspective provided by considering the state of the local ionosphere allows us to assess our findings within the context of a coupled M-I system.

Reliance on VLF waves has proven to be an effective tool for monitoring and characterizing the lower ionosphere (Sechrist, 1974; Inan et al., 2010; Gross and Cohen, 2020). Early research within the VLF band was focused on lightning-induced "sferics" (Pierce, 1969), a technique that formed the basis of modern lightning detection networks (Betz et al., 2009). VLF sferics can travel significant distances within the EIWG (Wait ans Spies, 1964) and be detected as sound "tweeks" due to the dispersive nature of the ionosphere (Singh et al., 2016). D-region characteristics can be derived from these events although some care is required to account for their sporadic nature, both temporally and spatially (McCormick and Morris, 2018). Conversely, controlled experiments using known VLF frequencies and transmitter-receiver great circle paths (TRGCPs) can be used to characterize the lower ionosphere nominally to and from fixed locations (Kumar and Kumar, 2020). Well-known features in VLF TRGCP propagation are diurnal variations in amplitude and phase (Yokoyama and Tanimura, 1933; Pierce, 1955; Taylor , 1960; Chilton et al., 1964; Lynn, 1978; Barr et al., 2000; McRae and Thomson, 2000; Sharma and More, 2017) and characteristic signatures of sunrise and sunset (Walker, 1965; Crombie , 1964, 1966; Ries, 1967; Samanes et al., 2015; Sharma and More, 2017; Gu and Xu, 2020). These features can be explained within the context of the wave-mode theory of VLF propagation attributed to Budden (1951, 1953, 1957) and promulgated by Wait Wait (1960, 1961, 1963, 1964, 1968, 1970) and collaborators (Spies and Wait, 1961; Wait ans Spies, 1964). While the transient response of VLF TRGCP propagation to solar flares has been well documented (Mitra, 1974; Thomson and Clilverd, 2001; McRae and Thomson, 2004; AbdRashid et al., 2013; Palit et al., 2013; Rozhnoi et al., 2019), the associated characterization to geomagnetic storms has been less quantified due, perhaps, to the mixed ionospheric responses in the lower atmosphere from geoeffective CMEs and CIRs (Turner et al. , 2006; Kim et al., 2008; Laughlin et al., 2008; Verbanac et al., 2011; Soni et al., 2020). The focus of this effort is then to augment the limited body of research related to the impact of geomagnetic storms on VLF propagation along TRGCPs within the EIWG (Tatsuta et al., 2015).

The ionospheric response to geomagnetic storms is varied and interpreting the response in terms of a regional or global specification of electron density often requires the use of sophisticated environmental models (Schunk et al., 2004; Immel and Mannucci, 2013; Greer et al., 2017). However, these models are mostly focused on the upper ionosphere, E-region and above, and inclusion of the D-region involves separate modules that, in turn, are mostly focused on the prompt D-region to solar transient events, in the forms of flares and related energetic particle events (Bilitza, 1998; Eccles et al., 2005; Sauer and Wilkinson, 2008; Rogers and Honary, 2014; Kulyamin and Dymnikov, 2016). The coupling between the dayside upper and lower ionospheric regions is tenuous as the electron density of the upper ionosphere is largely driven by solar EUV radiation whereas chemistry, mostly involving nitric oxide (NO), controls the quiescent D-region (Siskind et al., 2017). To facilitate the

development of improved D-region models the impacts of geomagnetic storms must be considered (Spjeldvik and Thorne, 1975; Dickinson and Bennett, 1978). Particularly germane to this present discussion is the impact of post-storm energetic particle precipitation (EPP) on the chemistry of the D-Region (Seppala et al., 2015; Rodger et al., 2015). Indices used to specify the D-region include the reflection height, H' (in km), and bottom-side profile sharpness, β (in km^{-1}), parameters originally developed by James Wait (Wait ans Spies, 1964) and commonly used in research applications (Thomson, 1993; Thomas et al., 2007; Nina et al., 2021) as well as operations involving VLF propagation within the EIWG (Nunn et al., 2004). Another pair of indices refer to the sunset D-Layer Disappearance Time (DLDT)) and the sunrise D-Layer Preparation Time (DLPT) associated with anomalous ionospheric behavior during geomagnetic storms (Choudhury et al., 2015) and earthquakes (Sasmal and Chakrabarti, 2009; Chakrabarti et al., 2010). Within this manuscript we choose to adopt a modified set of indices originally introduced by Nwankwo et al. (2016) which correspond to the mid-day signal amplitude peak (MDP), the mean signal amplitude before sunrise (MBSR) and mean signal amplitude after sunset (MASS). The use of these indices within the effort by Nwankwo et al. (2016) revealed trends, albeit inconsistent, in the signal strength of VLF radio waves propagating within the EIWG in response to several geomagnetic storms of moderate intensity. The intent of the current effort is to expand on the findings of Nwankwo et al. (2016) to further elucidate the effects of geomagnetic storms on the physics of the mid-latitude D-region. The following paragraphs review the status of geomagnetic storm related impacts on the high-, middle- and low-latitude D-region ionosphere (Lastovicka, 1996).

It was previously noted that solar Lyman alpha radiation is primarily responsible for maintaining the quiescent dayside D-region (Nicolet and Aikin, 1960) whereas flare-associated X-rays are the dominant D-region ionization source during solar flares (Thomson and Clilverd, 2001; Quan et al., 2021). Solar-flares are transient events which actively emit ionizing X-rays lasting for up to several tens of minutes (Veronig et el., 2002). A related class of solar transient is a solar particle event (SPE) resulting from an interplanetary CME-induced shock (Tsurutani et al., 2003; Mittal et al., 2011; Chandra et al., 2013; Dierckxsens et al., 2015; Gopalswamy, 2018), wherein charged particles, mostly protons, are accelerated to high energies and impact the lower atmosphere at the higher latitudes within the open magnetosphere (Zawedde et al., 2018). The precipitation of greater than 10 MeV solar energetic protons (SEPs) affects both the chemistry of the lower mesosphere (Ahrens and Henson , 2021), between 50 to 85 km (Turunen et al., 2009), and acts as a source of ionization that can temporarily increase the D-region electron density (Hunsucker, 1992; Sauer and Wilkinson, 2008; Neal et al., 2013). A sufficiently intense and energetic flux of SEPs can impact radio-wave communications in the form of a Polar Cap Absorption (PCA) event having a delayed onset following a solar flare, assuming the flare has a related CME, and a duration lasting for up to several days (Rose and Ziauddin, 1962; Potemra et al., 1970; Mitra, 1974; Rogers and Honary, 2014; Rogers et al., 2016). The Antarctic-Arctic Radiation-belt (Dynamic) Deposition-VLF Atmospheric Research Konsortium (AARDDVARK) network was established to probe the D-region with extreme sensitivity (Clilverd et al., 2009, 2014; Neal et al., 2015). An example of an early use of the AARDDVARK network was monitoring changes in the polar D-region from an SPE (Clilverd et al., 2007). Strictly speaking an SPE is quite distinct from a geomagnetic storm although they both have a common originating source. However, as it relates to our objective of better quantifying the D-region response to geomagnetic storms we are unaware of any efforts to separate

out the storm-specific responses from other, albeit related, sources.

195   During and following geomagnetic storms enhanced fluxes of energetic electrons from the outer van Allen radiation belts (van Allen et al., 1958) precipitate into the sub-auroral atmosphere (Peter et al., 2006) contributing to the formation of the storm-time mid-latitude D-region (Pedersen, 1962; Grafe et al., 1980; Horne et al., 2009; Zawedde et al., 2018; George et al., 2020). The nominal L-shell location (McIlwain, 1961) for the outer radiation belt is from L∼3 to L∼10 (George et al., 2020) which, for an idealized earth dipole field, maps to invariant latitudes of 54.80 and 71.60, respectively (Kilfoyle and Jacka ,

200   1968). The processes which regulate the electron populations within the outer belts during storm conditions are complicated and interdependent (Reeves and Daglis, 2016; Baker, 2019). An aspect not yet discussed is the fundamental role that aurora/magnetospheric substorms play in the dynamics of the magnetosphere (Akasofu, 1964; McPherron, 1979; Rostoker et al., 1980; Spence, 1996; Akasofu, 2020) and, germane to the topic at hand, the impacts on the mid-latitude D-region (Guerrero et al., 2017). A substorm is described as a "transient process initiated on the night side of the earth in which a significant amount

205   of energy derived from the solar wind-magnetosphere interaction is deposited in the auroral ionosphere and magnetosphere" (McPherron, 1979). This description is consistent with the concept of an open magnetosphere wherein the IMF and geomagnetic field lines merge at the dayside magnetopause and are then swept tailward with the solar wind into the nightside, or geotail, where the geomagnetic field lines and IMF respectively reconnect (Russell, 1991). When the IMF has a southward component the magnetopause standoff distance at noon is nominally located at about 10 earth radii (Re) (Aubry, 1970; Fairfield, 1971;

210   Shue et al., 1997; Suvorova and Dmitriev, 2015; Bonde et al., 2018; Samsonov et al., 2020). During a geomagnetic storm the magnetopause can be significantly "eroded" (Wiltberger et al., 2003; Le at al., 2016) reducing the location of the standoff distance which may be within the geostationary orbit of 6.7 Re under extreme conditions (Shue et al., 1998). In response to the storm, the polar-cap potential and the cross-tail current increase as energy is continually transferred from the solar wind into the geotail (Angelopoulos et al., 2020). While it is curious that the electron density within the outer radiation belt can either

215   increase or decrease under storm conditions (Reeeves et al., 2020) more relevant to establishing (nightside) or maintaining (dayside) the ionospheric D-region is that the electrons within the outer belt can be pumped up to extremely high, including relativistic, energies by local wave activity and radial diffusion (Baker, 2019; Kanekal and Miyoshi, 2021). A fraction of these energetic electrons can be subsequently scattered into the atmospheric loss cone (Porazik et al., 2014) by naturally occurring electromagnetic waves (Spjeldvik and Thorne, 1975; Gu et al., 2020; Ripoll et al., 2020; Aryan et al., 2021) and precipitate

220   into the lower ionosphere at mid-latitudes where they collisionally ionize the neutral atmospheric constituents (Rodger et al., 2007, 2010, 2012; Naidu et al., 2020). The outer radiation belt can relax to its more quiescent state on time scales ranging from minutes (Turner et al., 2013) to many days (Baker, 2019) following a significant geomagnetic storm. It should be noted, in conclusion, that although the evidence provided herein shows a clear association of magnetic storms with enhanced levels of electron precipitation it is likely that even during geomagnetically quiet intervals electron precipitation persists but apparently

225   at a greatly reduced rate (Mironova et al., 2021).

As previously discussed, Appleton and contemporaries (Colwell and Friend, 1936) in the early 1900's used short-distance VLF radio-wave transmissions to probe and study the D-region whereas the efforts of Wait and colleagues (Wait ans Spies, 1964) were to facilitate global VLF communications within the EIWG. The early work to quantify storm-related D-region impacts involved the general technique of HF radio-wave absorption (Eccles et al., 2005; Pederick and Cervera, 2014; Scotto and Settimi, 2014; Siskind et al., 2017). In this regard Lauter and Knuth (1967) found that the aftereffects of geomagnetic storms on the absorption of 245 kHz radio waves in the mid-latitude D-region could persist for more than 10 days. Supporting in-situ rocket data (Dickinson and Bennett, 1978) revealed that the electron density in the days following an "intense" geomagnetic storm could be 4 to 10 times the normal daytime density and that these measurements were well correlated with changes in HF radio-wave absorption. An interesting finding by Satori (1991) was the countering effect of a Forbush decrease on the density of the D-region at mid-latitudes. A Forbush decrease refers to the measured reduction in the galactic cosmic ray background due to an earth-passing CME (Forbush, 1954; Raghav et al., 2020; Janvier et al., 2021). Cosmic rays are an important D-region ionization source at night and a minor contributor during the day (Moler, 1960). According to Satori (1991), the reduction in the galactic cosmic ray flux associated with a CME counters the increased D-region ionization from precipitating radiation belt electrons during a geomagnetic storm.

Again, the focus of this report is on the geomagnetic storm-related impacts to VLF TRGCP radio-wave propagation and the information on the D-region that can be gleaned from this approach. In this regard (Belrose and Thomas, 1968) reported that VLF amplitudes during a geomagnetic storm were unaffected whereas phase measurements showed rapid fluctuations with residual effects lasting several days following the storm. Muraoka (1979) found that the prevalence of these phase anomalies was dependent on the strength of the magnetic storm. Upon further examination, as reported by Rodger et al. (2007), both signal amplitude and phase variations in VLF TRGCP transmissions were found to be sensitive to electron precipitation events during geomagnetic storms. Choudhury et al. (2015) found that receiver position electron density was the main controlling factor in their storm-time metric of the sunrise DLPT depth in VLF TRGCP radio-wave propagation. This metric plus the MDP parameter (after Nwankwo et al., 2016) were used by Naidu et al. (2020) to ascertain, again, that geomagnetic-storm related impacts to the D-region were due to energetic electron precipitation. Recently Kerrache et al. (2021) clarified the role of lightning-induced electron precipitation (LEP) events (Voss et al., 1998; Blake et al., 2001; Inan et al., 2010) in the pitch angle scattering of outer radiation belt electrons during geomagnetic storms and their impact on VLF TRGCP transmissions within the EIWG.

The mechanisms that affect the low-latitude D-region in response to geomagnetic storms have not been extensively studied and are still relatively unknown (Araki, 1974; Kleimenova et al., 2004; Kumar and Kumar, 2014; Kumar et al., 2015; Maurya et al., 2018). It is recognized that the low-latitude E- and F-region ionospheres can be affected by storm-induced prompt penetration electric fields (PPEFs) (Tsurutani et al., 2008; Timocin, 2022) and disturbance dynamo electric fields (DDEFs) (Blanc and Richmond, 1980; Fejer et al., 1983; Scherliess and Fejer, 1997) plus related substorm effects (Sastri, 2006; Chakraborty et al., 2015; Hui et al., 2017). Generally speaking, PPEFs refer to the immediate and sustained fields resulting from the active

response of the magnetosphere to an externally imposed forcing function such as a CME-induced shock (Nava et al., 2016), whereas DDEFs result from the delayed equatorward motion of the thermosphere in response to auroral heating and chemistry (Zesta and Oliveira, 2019; Robinson and Zanetti, 2021). Transient substorms affect the dynamics of the low-latitude iono-sphere as the magnetotail attempts to accommodate an increased storm-time reconnection rate (Hajra, 2021). However, these storm-time perturbations do not appear to affect the lower ionosphere except under the most extreme situations. For example, in a limited study of 7 moderate (Dst < -50) to intense (Dst < -100) geomagnetic storms Kumar and Kumar (2014) found that only the intense storm of 16 Dec 2006, with a Dst = -145, had a clear measurable effect on VLF TRGCP transmissions at low latitudes. These finding are consistent with early studies (Araki, 1974) on the effects of large storms on trans-equatorial VLF propagation. Other case studies of intense (Kumar et al., 2015; Maurya et al., 2018) to super (Dst < -200, Wu et al., 2016) geomagnetic storms validate this D-region response although the specific mechanisms for coupling the low-latitude D-region ionosphere to the higher latitudes in terms of gravity waves or chemical processes have not yet been confirmed.

We have provided an extensive and, hopefully, well documented background on the use VLF radio waves to probe the ionospheric D-region with an emphasis on the impacts of geomagnetic storms. Monitoring VLF radio-wave propagation within the EIWG along TRGCPs is a convenient and cost-effective technique for determining how space weather affects this lowest traditional ionospheric density layer. While the D-region is an important enabling element for VLF communications, it is also an interface linking the middle atmospheric regions to the upper ionosphere. We have stressed the role of the D-region within an M-I perspective of a driven system during geomagnetic storms perhaps at the expense of expanding on the impacts to and the feedback from the neutral atmosphere. While much of the basic physics and chemistry of the D-region is well understood how geomagnetic storms affect this region of space remains an active area of research. Our goal within this manuscript is to contribute in some small way to the existing body of knowledge concerning the D-region as it pertains to VLF radio-wave propagation. Therefore, we (in this study) combine the observed diurnal VLF amplitude variation in the D-region with standard measurements of the E and F regions to perform a diagnostic investigation of coupled geomagnetic storm effects, in order to understand the observed storm-induced variations in VLF narrowband based on the state and responses of ionosphere.

2   Data and Method

We obtained the VLF amplitude data for DHO-A118 and GQD-A118 propagation paths received at A118 SID monitoring station in Muret, Southern France (lat N43.53° long E1.39°). The location of the transmitters (GQD (22.1 kHz GQD, lat N54.73° long W002.88°) and DHO (23.4 kHz, lat N53.08° long W007.61°)) and the receiver (A118) are shown in Figure 1. The DHO and GQD transmitters and the A118 receiver are 1169.18 km and 1315.66 km, respectively. Other data include GOES solar X-ray flux, solar wind speed (V_{sw}) and particle density (PD) (ftp://sohoftp.nascom.nasa.gov/sdb/goes/ace/), planetary geomagnetic A_p and the Dst index (from World Data Centre for Geomagnetism (WDCG)). These data were described in detail in Nwankwo et al. (2016) and references therein.

Figure 1. VLF signal propagation paths (DHO-A118 and GQD-A118) used in the study

295   The analysed storm intervals are 16th-31st September and 22 October-5 November 2011, while the geomagnetic storms of interest within the intervals include the events on 17, 26-27 September, 25 October and 1 November 2011. We monitor variation 2-4 hour mean VLF signal amplitude before local sunrise and after sunset (hereafter respectively denoted as MBSR and MASS), and the mid-day signal amplitude peak (MDP). We note that the acronym DTMA (daytime mean amplitude) was used in Nwankwo et al. (2021) instead of the MDP. The difference between the two metrics is that DTMA represent

300   1-hour mean value of the signal amplitude around midday, while MDP is the value of the signal amplitude at midday. We also identified typical values of the signal at sunrise and sunset, also recognised as sunrise and sunset terminators (hereafter, denoted as SRT and SST). When propagating in the EIWG VLF signal amplitude and phase responds to dynamic conditions in the ionosphere such as variation in the reflection height and/or width of the EIWG caused by changes in ionization rate. VLF/LF also response to other solar-induced phonomena (e.g., SID, solar eclipse and geomagnetic stormes-induced energetic particle

305   penetration) as well as non-solar phenomena (e.g., gravity waves, lightening) (Silber and Price, 2017) as extensively discussed in the introduction section. In addition to the diurnal variation of the ionosphere, the received signal also reflects the state of the traversed region of the ionosphere between the transmitted and the receiver (Nwankwo et al., 2020b). Therefore, monitoring the trends in variation of all these metrics enabled us study the response of the VLF radio waves to geomagnetic storms as they pertain to the induced ionospheric pertubations in the waveguide and the diurnal signature or variation in amplitude. The

310   diurnal VLF amplitude indicating portion of the characterised metrics (MBSR, MDP, MASS, SRT and SST) are shown in Fig. 2a. The signals were analysed in conjunction with geomagnetic indices, to describe storm-induced magnetosphere-ionosphere coupling in mid-latitude D region. We thus study the trend in variations of these key metrics under varying geomagnetic storm conditions using the signal propagation characteristics, to understand behaviours attributable to geomagnetic storm-induced variations in the lower ionosphere (besides the visible response of the signal's amplitude and/or phase to solar flare induced

315   X-ray flux).
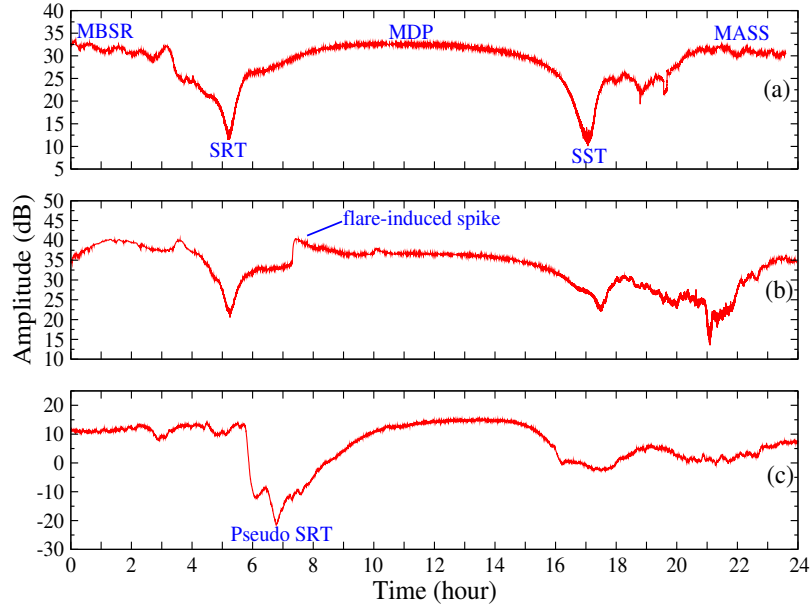
Figure 2. Diurnal VLF signal amplitude signatures (from DHO-A118 propagation path) showing analysed signal metrics

3 Results and Discussion

3.1 Analysis of VLF amplitude variations during intervals of geomagnetic storms

Figure 3 shows the diurnal variation in VLF amplitude for (a) DHO-A118 and (b) GQD-A118 propagation paths, daily variation in (c) X-ray flux output (d) solar wind speed (V_{sw}) (e) solar particle density (PD) (f) Dst (g) planetary geomagnetic A_p and (h) Auroral Electrojet (AE) indices during 16-30 September 2011. Four storm conditions were recorded during the period; moderate storm on 17th (Dst=-60) and consecutive storms on 26th (Dst=-101), 27th (Dst=-88) and 28th (Dst=-62), presumably driven by the significant increase in V_{sw} and PD on 17th and 26th (Fig. 3a-f). However, the main reference storms are those of 17th and 26th. The variation of the AE (especially between 26th and 29th) appear to be consistent with storm related high-intensity, long-duration continuous AE activity events (HILDCAAs). Hence, 'fresh energy was injected' into the magnetosphere in the process (Tsurutani et al., 2011). We observed a notable drop in DHO-A118 VLF signal level on 26th around midday following the relatively intense storm condition with Dst up to -101 (Fig. 3a). This scenario (signal strength decrease) have been associated with storm-induced variations in energetic electron precipitation flux (Kikuchi and Evans, 1983; Peter et al., 2006). During a geomagnetic storm, the current system in the ionosphere, and the energetic particles precipitate into the ionosphere can influence the density and distribution of density in the atmosphere (NOAA4, 2016). The characterised metrics (e.g., MBSR, MDP, MASS, SST and SRT) of the VLF signal amplitude makes it easier to study the behaviour of the signal during the storms by monitoring their trends of variation. We therefore monitor trends of the signals variation in the analysis
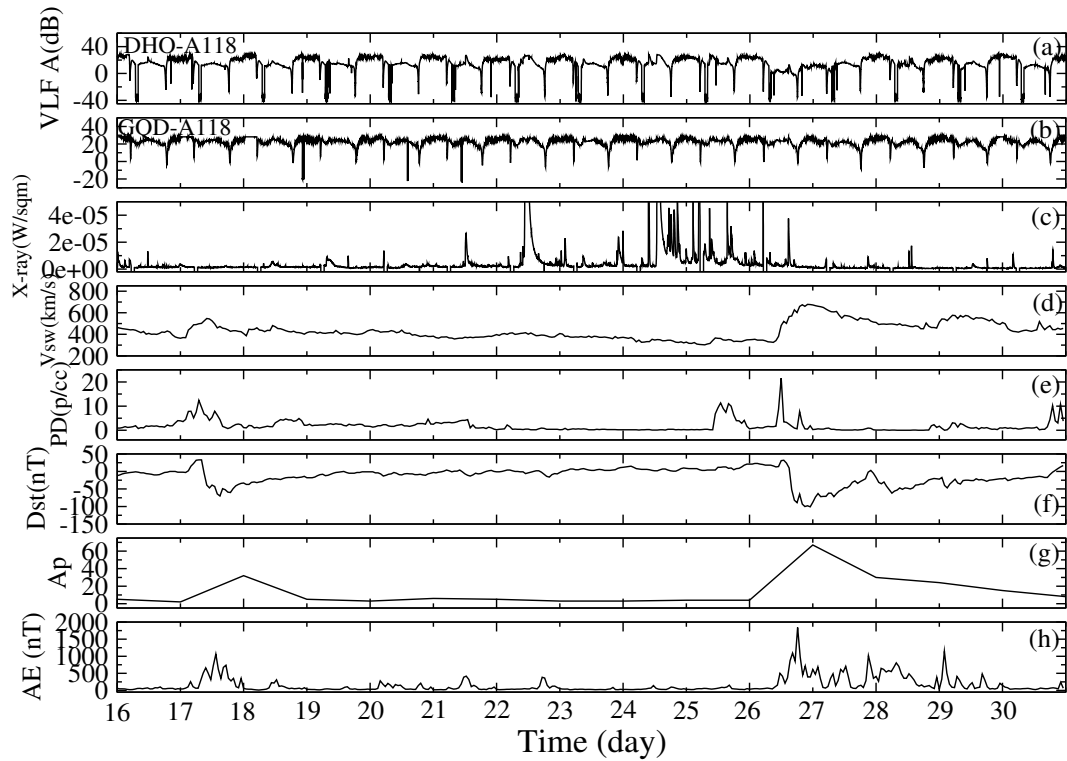
Figure 3. (a) Diurnal VLF amplitude for DHO-A118 and (b) GQD-A118 propagation paths (c) daily variation in X-ray flux output (d) solar wind speed (V_{sw}) (e) solar particle density (PD) (f) Disturbance storm time (Dst) (g) planetary A_p and (h) Auroral Electrojet (AE) indices during 16-30 September 2011

to follow for possible identification of storm-induced variation in the signal due to lower ionosphere responses.

Figure 4 shows daily mean fluctuation of Dst and AE, and variations in the VLF midday signal amplitude peak (MDP), mean signal amplitude before local sunrise (MBSR), mean signal amplitude after sunset (MASS), sunrise terminator (SRT) and sunset terminator (SST) for (a) DHO-A118 and (b) GQD-A118 propagation paths during 16-30 September 2011. In GQD-A118 propagation path (Fig. 4a), we observed a dipping of the MDP on 17th (extending to 20th), as well as dipping of the MASS on 17 Sept., but an increase of the MBSR, SRT and SST. Following the recurrent storms between 26 and 28 Sept., we observed dipping of the MDP on 26 Sept (extending to 29th). The slight increase of the signal (MDP) on 28th appear to be due to the significant flare activity (3 C-class and M-class), suggesting increase in both the instantaneous and background X-ray flux output that usually results to spike in signal amplitude (as depicted in figure 2b). High flare activity can 'overshadow' the signal's response to geomagnetic storms when the event coincide with storm time (Nwankwo et al., 2016). There is also a significant dipping of all the signal metrics (MDP, MBSR, MASS, SRT and SST) on 27 Sept. We note dipping of the MBSR on the days following the main (reference) storms on 18 and 27 Sept. Since the events occurred after dawn (around midday),
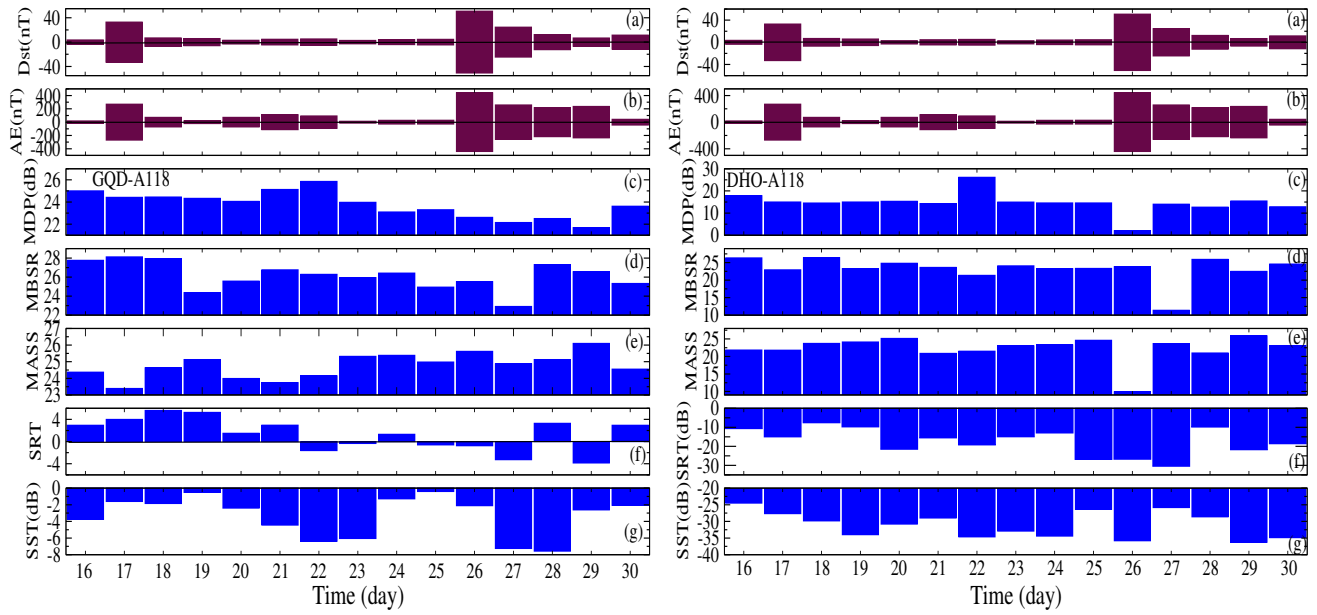
Figure 4. Daily deviations of (a) Dst (b) AE (c) variations in the peak value of midday signal amplitude (MDP) (d) mean signal amplitude before local sunrise (MBSR) (e) mean signal amplitude after sunset (MASS) (f) variation in sunrise terminator (SRT) and (g) sunset terminator (SST) for GQD-A118 (left panel) and DHO-A118 (right panel) propagation paths during 16-30 September 2011.

the post-storm ionospheric effects are expected well into the day following the storm. This trend (post-storm day signal dip), suggest that the signals dipped in response to continuous driving of the ionospheric on the days following the events. However, such response also depend on the characteristics of the signals propagation path. In DHO-A118 propagation path, dipping of the MDP, MBSR, SRT and SST occurred on 17 Sept., and only the MDP, MASS and SST decreased on 26 Sept. The MASS and SRT maintained the pre-storm day values of 16 and 25 Sept., respectively. While the MBSR increased slightly on 26th (main storm day), there is a significant dipping of the signal following recurrent storm of 27 Sept.

Figure 5 shows diurnal VLF amplitude for (a) DHO-A118 and (b) GQD-A118 propagation paths, daily variation in (c) X-ray flux output (d) V_{sw} (e) PD (f) Dst (g) A_p and (h) AE indices during 22 October - 5 November 2011. This period is associated with a severe storm with main phase on 25th October (Dst=-132) and consecutive storms on 1 November (Dst=-71) and 2nd November (Dst=-57), presumably driven by the highly variable V_{sw} and PD (Fig. 5d-e). It has been shown that the capability of a given value of the solar wind electric field (SWEF) to create a Dst disturbance or geo-efficiency is enhanced by high solar wind density (Weigel, 2010; Tsurutani et al., 2011). Variation of the AE between 30 Oct. and 3rd Nov. also appear to be consistent with HILDCAAs (Fig. 5h). The DHO-A118 VLF signal level on 25 October around midday also showed a visible reduction following the intense storm condition with Dst up to -132 (Fig. 5a). VLF signal data for GQD-A118 propagation
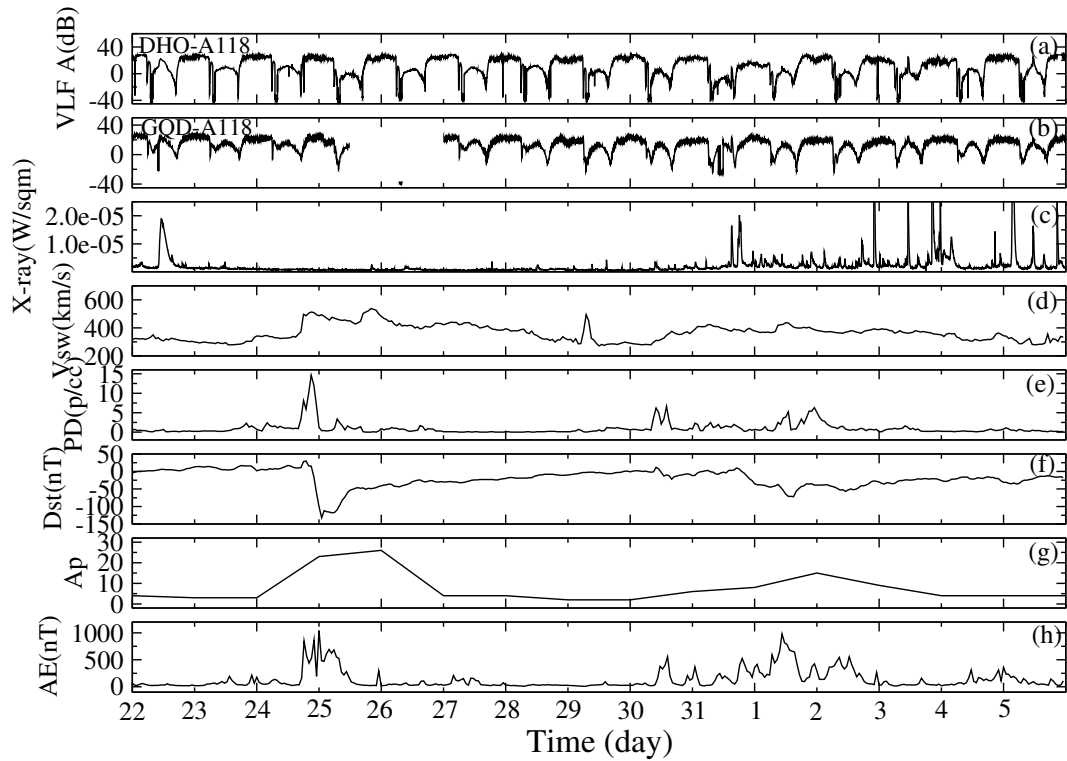
Figure 5. (a) Diurnal VLF amplitude for DHO-A118 and (b) GQD-A118 propagation paths (c) daily variation in X-ray flux output (d) solar wind speed (V_{sw}) (e) solar particle density (PD) (f) Disturbance storm time (Dst) (g) planetary A_p and (h) Auroral Electrojet (AE) indices during 22 October to 5 November 2011

360 path are not available during 12:00 noon, 25 Oct. to 06:00 pm on 26th October (Fig. 5b).

Figure 6 shows daily deviations of Dst and AE, and variations in the MDP, MBSR, MASS, SRT and SST for (a) DHO-A118 and (b) GQD-A118 propagation paths during 22 October - 5 November 2011. Although data for GQD-A118 propagation path during 25 and 26 October is inadequate for the present analysis, we did observe a dipping of the MBSR on the main storm day

365 (25 Oct.). Dipping of the MDP, MASS and SST occurred on 1 Nov., and those of MBSR, MASS, and SRT on 2 Nov., following the consecutive storms. In DHO-A118 propagation path, we observed dipping of the MDP, MBSR, MASS, and SRT on 25 Oct., dipping of the MDP, MBSR, MASS, and SST on 1st Nov., and dipping of the MBSR and SRT on 2 Nov. Similar to the first case (Figs. 4 and 5), we note the high flare events on 2nd Nov (up to 7 C-class and M-class), that may have induced a spike in the MDP on the day in both GQD-A118 and DHO-A118 propagation paths. Although dipping of the MDP signal (following

370 storm events) has shown a considerable consistency across the cases presented so far, the MBSR and MASS (in particular) appear to be influenced by storms occurrence time and the high variability or fluctuation of the dusk-to-dawn ionosphere (and signal) (Nwankwo et al., 2016). However, presenting a consistency across a substantial number of cases is vital to the conclu-
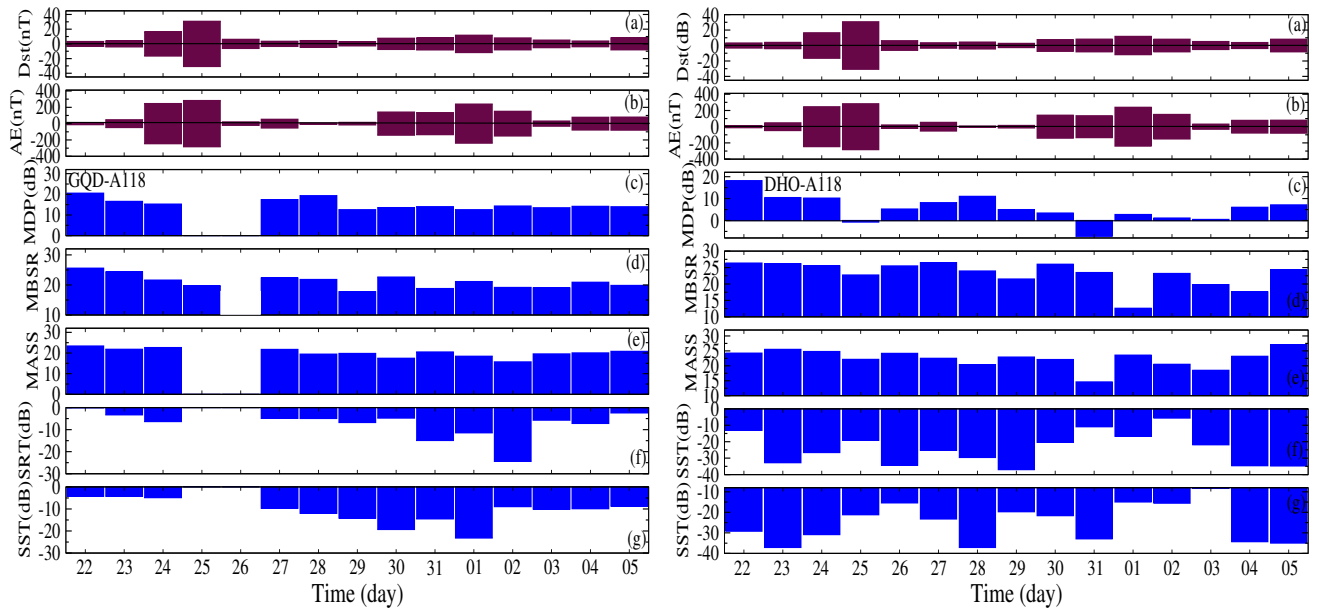
Figure 6. Daily deviations of (a) Dst and (b) AE (c) variations in MDP (d) MBSR (e) MASS (f) SRT and (g) SST for GQD-A118 (left panel) and DHO-A118 (right panel) propagation paths during 22 October - 5 November 2011.

sion of this work. We, therefore, statistically analyze 15 more storm cases between September 2011 and October 2012 in order to obtain the statistical significance of the observations. The 15 storm cases are presented in Table 1, which excluded some cases that were previously analysed in Nwankwo et al. (2016) but also with addition of new cases.

In Figure 7, we show Dst deviations (σ_{Dst}) and trend in variation of the MDP, MBSR, MASS, SRT and SST signals on the day before the storm (blue bar), the storm day (red bar) and after the storm day (brown bar) for the 15 selected storm cases in (a) GQD-A118 and (b) DHO-A118 propagation paths. σ_{Dst} is the measure or extent of daily fluctuation in measured values of Dst. We recognised the 3 consecutive days as day before event (BE), during event (DE) and after event (AEv). A '0' indicate absence of data. It should be noted however (for this analysis) that these events are separate events, and not continuous events. In GQD-A118 propagation path, about 8 of 12 MDP, 10 of 13 MBSR, 7 of 12 MASS, 3 of 12 SRT and 5 of 12 SST showed dipping features, while 12 of 15 MDP, 9 of 15 MBSR, 10 of 15 MASS, 5 of 15 SRT and 7 of 15 SST showed dipping in DHO-A118 propagation path. These values correspond to 67%, 77%, 58%, 25% and 42% dipping in GQD-A118 propagation path and 80%, 60%, 67%, 33% and 47% dipping in DHO-A118 ptopagation path. The signal levels, along with the percentage dip are presented in Table 2. The MDP signals (in both propagation paths) have generally shown remarkable evidence of dipping following geomagnetic storm conditions. However, we did also observe few cases of increase of the MDP during separate events in both propagation paths (e.g., events 4 and 7 in GQD-A118 and 9 in DHO-A118), as well as increase occurring in both propagation paths during same event (e.g., events 3 and 12). While the probable reason for the observed scenario is

Table 1. Summary of analysed 15 geomagnetic storm events

No.	Date	Max Dst (nT)	σ_{Dst}	Flare count(C M X)
1	26092011	-101	±50.73	9 2 0
2	25102011	-132	±30.76	1 0 0
3	22012012	-67	±37.00	4 0 0
4	15022012	-58	±9.63	0 0 0
5	19022012	-54	±12.8	1 0 0
6	07032012	-74	±25.41	1 0 0
7	15032012	-74	±20.75	1 0 0
8	28032012	-55	±12.09	1 0 0
9	05042012	-54	±13.82	3 0 0
10	23042012	-95	±32.23	3 0 0
11	12062012	-51	±12.47	13 0 0
12	16062012	95	±20.24	4 0 0
13	15072012	-126	±47.88	8 0 0
14	02092012	-54	±13.86	5 0 0
15	09102012	-105	±25.64	10 1 0

suggestive of factors such as propagation characteristics and/or X-ray flux induced spike in amplitude (e.g., significant X-ray output during event 3 and 7 in fig 8c), further investigation into why this characteristic exist will be pursued. In the mean time, we analyze variations in X-ray flux output and geomagnetic indices during events 3 and 12 to better interpret the prevailing ionospheric conditions at the time.

Table 2. Summary of trend in dipping of the signals' metrics during 15 geomagnetic storm case in (a) DHO-A118 and GQD-A118 propagation path

Signal (dB)	GQD-A118 propagation path			DHO-A118 propagation path		
	Available data	No. of dips	% dip	Available data	No. of dips	% dip
MDP	12	8	67	15	12	80
MBSR	13	10	77	15	9	60
MASS	12	7	58	15	10	67
SRT	12	3	25	15	5	33
SST	12	5	42	15	7	47

In Figure 8, we show the diurnal VLF amplitude for (a) DHO-A118 and (b) GQD-A118 propagation paths, daily variation in (c) X-ray flux output (d) V_{sw} (e) PD and (f) Dst indices for a day before and after each of the 15 storms condition. Data showed (Fig. 8c, Fig. 8f) the occurrence of M-class flare in association with the storm on 22-23 January 2012 (event 3 on 21 January), both events having near-corresponding peaks. This scenario suggest an enhancement of both the instantaneous and
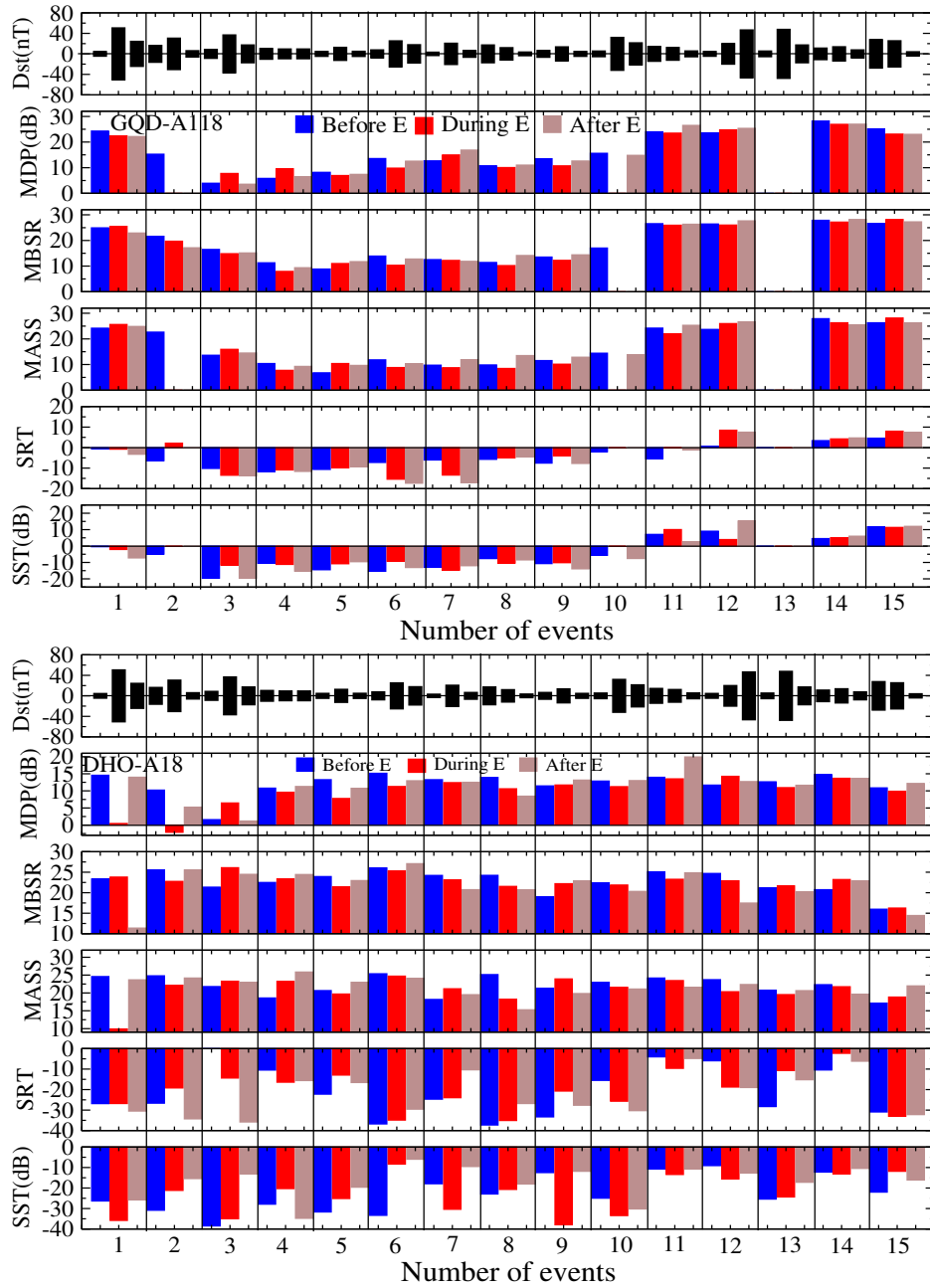
Figure 7. Dst deviation (or fluctuation), and variations in MDP, MBSR, MASS, SRT and SST signals 1-day before, during and after each of the 15 events for GQD-A118 and DHO-A118 propagation paths. Note that the each Dst bar represent the deviation (σ) corresponding to the VLF amplitude before, during and after the selected events (storm) as listed in Table 1 and shown in figure 8. The events are selected (for the intervals shown in fig 8) and not continous
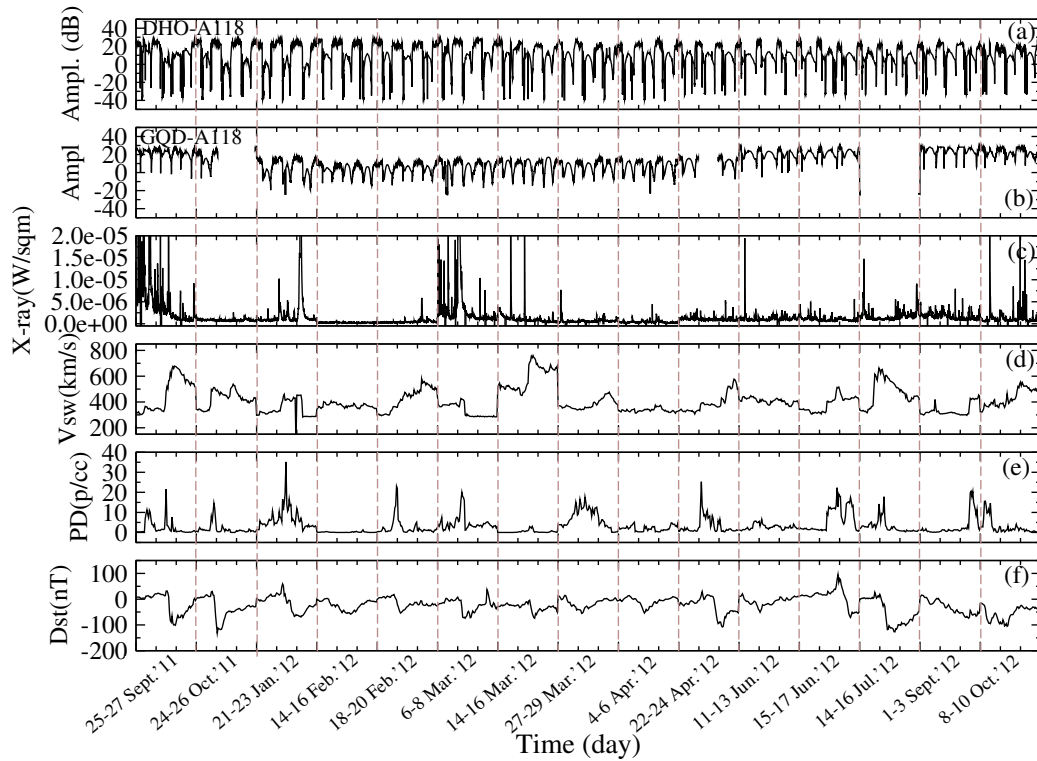
Figure 8. Diurnal VLF amplitude for (a) DHO-A118 and (b) GQD-A118 propagation paths, daily variation in (c) X-ray flux output (d) V_{sw}, (e) PD and (f) Dst indices for a day before and after each of the 15 storms

background X-ray flux output (as stated earlier), that may have caused increase (or, spike) in the signal level. Thus probably
400 overshadowed geomagnetic effects on the signal. While this explanation may be argued for events 1 (25-27 Sept. 2011) and
6 (6-8 Mar. 2012), it should be noted that the flare events started well before the storms, and continued until the storms time
(in each case), suggesting an established increase in the overall background X-ray before the storms. Hence, it is possible for
a storm-induced dipping to manifest under such condition. However, further investigation is encouraged, which is beyond the
scope of this work. For event 12 (during 15-17 July 2012), we observed that the peak of the storm (that commenced by mid-
405 night on 16th) was on 17th (recognised as AEv). Therefore, any geomagnetic influence on the signal (e.g., dipping) is expected
on 17th (or, after) and not 16th, hence the dipping of the AEv signal (on 17 Sept.) instead in DHO-A118 propagation path.

Figure 9 shows Dst deviation (fluctuation) and 2-day mean variations of MDP, MBSR, MASS, SRT and SST signals before,
during and after each event for (a) GQD-A118 and (b) DHO-A118 propagation paths. This analysis is important for corrobo-
410 rating the result presented in Figure 7, because the data selection criteria differ from those of Figure 7 in some ways. While BE,
DE and AEv represent data for three consecutive days with reference to the event's day (DE) in the former analysis (presented

in Fig. 7), each acronym (BE, DE or AEv) represent relatively quiescent 2-day mean amplitude before and after DE (but not necessarily in succession to/after DE). However, it should be noted that due to the data averaging (2-day), a 'pronounced' increase or dipping in the signals (comparable to those in the former analysis (fig 7)) are not expected. Another important data selection criterion for this analysis is a relative geomagnetic quiet day BE and AEv with respect to DE.

In GQD-A118 propagation path, 7 of 12 MDP, 7 of 13 MBSR, 7 of 12 MASS, 6 of 12 SRT and 3 of 12 SST showed dipping following the storms, while 10 of 15 MDP, 11 of 15 MBSR, 11 of 15 MASS, 6 of 14 SRT and 6 of 15 SST showed dipping in DHO-A118 propagation path. These values correspond to respective 58%, 54%, 58%, 50% and 25% dipping in GQD-A118 propagation path and 67%, 73%, 73%, 43% and 40% dipping in DHO-A118 propagation path. The signal levels, along with the percentage dip of the signals are presented in Table 3. In general, the trend of variation of the signal metrics considerably reflected the prevailing space weather-coupled effects in the lower ionosphere. The MDP signal appears to be more responsive to geomagnetic perturbations (58% and 67% (67% and 80% for 1-day mean analysis) in respective popragation paths shown in figs 7 and 9) than other signal metrics. However, the 2-day mean analysis showed improvement in MBSR and MASS (73%) the DHO-A118 propagation path, thereby reenforcing the responsiveness of this propagation path to geomagnetic storm impacts. While the mechanism of VLF amplitude (and/or MDP) response to flare-induced SIDs is well understood (see, section 1.3 of (Nwankwo et al., 2016)), the mechanism of the transient response of the signal to geomagnetic storm is not well developed. We speculate that the dipping response of the MDP may be related to (i) positive storm effect, which affects, albeit small, the attenuation of the VLF radio waves (Fagundes et al., 2016) (ii) adjustment of the D layer to storm driven energy input (McPherron, 1979) (iii) precipitation of energetic electrons (Rodger et al., 2010, 2012; Naidu et al., 2020) and/or (iv) charge exchanged between surrounding ionospheric regions (Tatsuta et al., 2015). Since the processes are gradual (when compared to SID scenario) and originating from the magnetosphere, it is not likely that a remote spike occur in the diurnal signal (as observed during flare condition). One other likely reason for the observed dipping characteristic is the modification of the chemistry of the D region by storm pricipitation of SEPs (Turunen et al., 2009), since chemistry (mainly NO) controls the quiescent D-region (Siskind et al., 2017).

Nwankwo et al. (2016) noted the existence of pseudo-SRT and SST exhibited by diurnal VLF signal (see, Fig. 2c) as drawback in SRT and SST analysis. This anomaly is due to secondary destructive interference pattern in signals and occurrence of solar flares during sunrise/sunset (Chakrabarti, personal com., 2016). Authors concluded in their study that the post-storm SRT and SST variations do not appear to have a well-defined trend associated with storm effect based on the approach used in the analysis (Nwankwo et al., 2016). In this work, we considered the 'first' SRT and SST values (in the event of a pseudo-terminator) during analysis of the signal metrics. A rise in SRT and SST amplitude under geomagnetic storm conditions appear to occur more than otherwise in both propagation paths. We found a respective dipping of 50% and 25% (43% and 40%) of the SRT and SST. Storm-induced disturbances may not have significant influence on these metrics (SRT and SST), and since the sunrise and sunset signatures relates to mode conversion in the VLF propagation path it might imply that the D-region density is not a significant contributor to this effect. It is important to note that of the two propagation paths used in this study, the
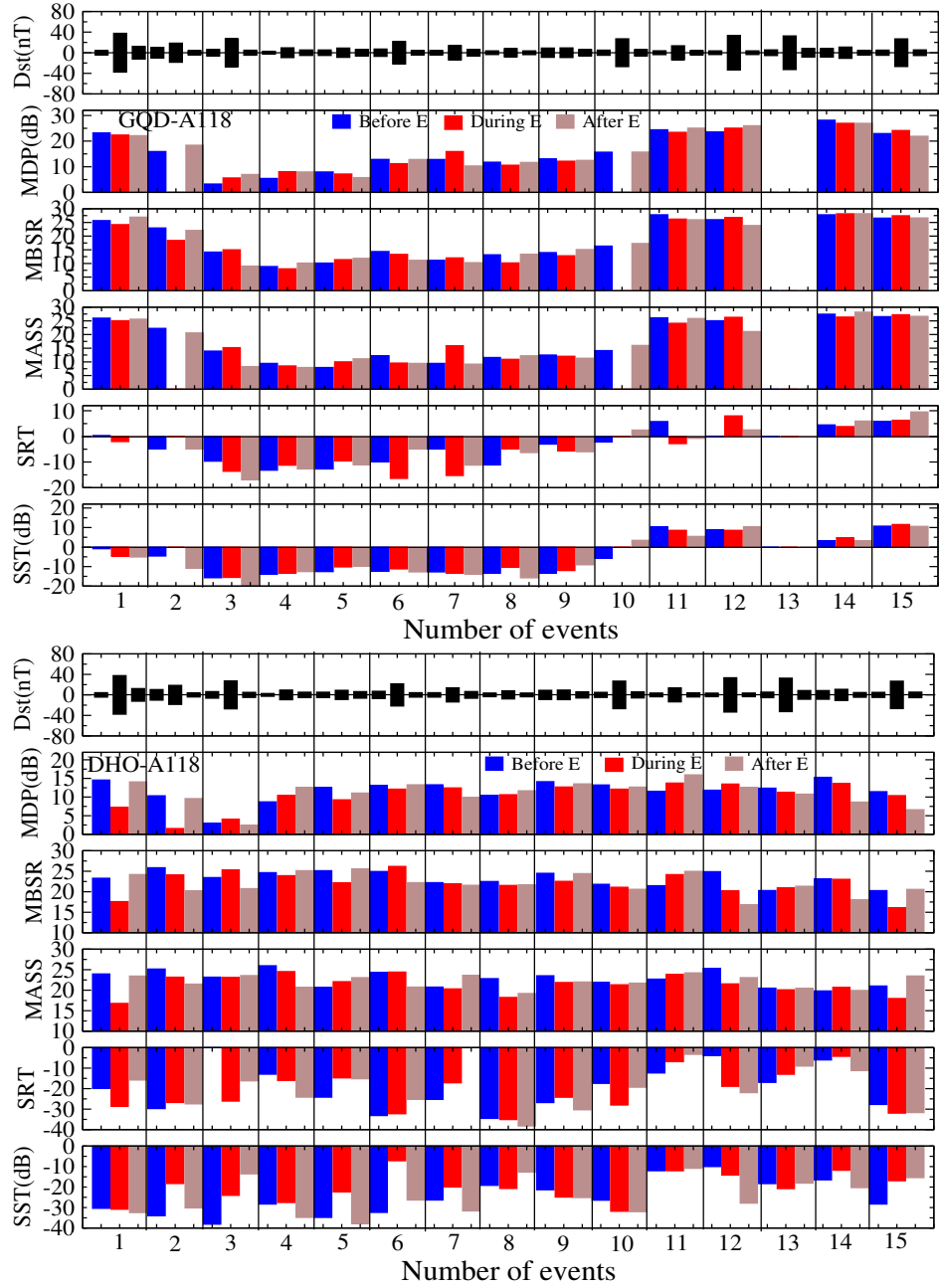
Figure 9. Dst deviation and 2-day mean variations of MDP, MBSR, MASS, SRT and SST signals before, during and after each event for GQD-A118 and DHO-A118 propagation paths.

DHO-A118 signal appears to be more sensitive to geomagnetic storm-induced magnetosphere-ionospheric dynamics. We do not expect a 'perfect' consistency in signal trend and variations across all cases, because the individual effects of solar and other forcing mechanisms (including those of lithospheric and atmospheric sources) on the ionosphere are difficult to estimate (Kutiev, 2013; Nwankwo et al., 2016). This scenario can also cause non-linear coupling processes and consequent significant fluctuations in radio signals.

Table 3. Summary of trend in 2-day mean signals dipping following 15 geomagnetic storm case in (a) DHO-A118 and GQD-A118 propagation path

Signal (dB)	GQD-A118 propagation path			DHO-A118 propagation path		
	Available data	No. of dips	% dip	Available data	No. of dips	% dip
MDP	12	7	58	15	10	67
MBSR	13	7	54	15	11	73
MASS	12	7	58	15	11	73
SRT	12	6	50	14	6	43
SST	12	3	25	15	6	40

3.2   Investigating the state of the ionosphere over the propagation paths of the VLF signals

Here, we study the state of the ionosphere over the two VLF propagation paths using the virtual heights (h'E, h'F1 and h'F2) and critical frequencies ($f o$E, $f o$F1, and $f o$F2) of the E and F regions obtained from two ionosonde stations near the GQD and DHO transmitters. Although we made effort to obtain data from stations near each transmitter/receiver and at the mid-point, we found no ionosonde station at the mid-point, and the nearest station to the receiver (Tortosa) has no data for the period/intervals under study. However, to make up for this dearth of data, we will complement the analysis with the results in the extended study that utilised the GNSS data in the region (e.g., (Nwankwo et al., 2021)). Details of the ionosonde stations used in this study are provided in Table 4. We treat Chilton station as nearest to GQD transmitter and Juliusruh station nearest to DHO transmitter. Tortosa station is closest to the A118 transmitter but has no data for the intervals. We obtained and calculated the daytime (8:00 am - 3:00 pm) mean values and standard deviations (σ) of the parameters, and analyzed for the storms of interest (on 17 and 26 September and 1 November) within the intervals 16-19, 25-28 September and 29 October to 2 November 2011. We exclude analysis of the 25 October storm because the data for this interval are inadequate.

Figure 10 shows the daily mean and standard deviation (SD or σ) of foF2, foF1, foEs, foE, h'F2, h'F, h'Es and h'E during 16-17 September 2011 for Chilton and Juliusruh Stations. We compare the pre-storm day (blue broken line) values with the storm day (red broken line) values. At Chilton station (near the GQD transmitter) result show significant increase and/or fluctuation (increase in SD) of the foF2, and a decrease (with significant fluctuation) of foF1 on the storm day, 17 September. The height of the E and F regions (h'F2, h'F, h'Es and h'E) significantly increased following the storm. Similar pattern of variations were observed at Juliusruh station. The foF2 and foF1 increased (and/or fluctuated) significantly, as well as h'F2,

Table 4. Ionosode stations near the VLF transmitters, receiver and/or propagation paths

Station	Location	Coordinate	Nearest Transmitter/Receiver	Approx. dist. from Transmitter/Receiver
Chilton	United Kingdom	51.5696°N, 1.2997°W	GQD	394.15 km
Juliusruh	Germany	54.6207°N, 13.3719°E	DHO	415.71 km
Tortosa	Spain	40.8126°N, 0.5214°E	A118	301.87 km

h'F, h'Es and h'E. Values of foEs decreased, while the foE remained unaffected in both stations. Also, there appear to be a sustained post-storm increase and/or fluctuations of the parameters on on 18 September, suggesting a continuous driving of the ionosphere by the storm.

475   Figure 11 show the daytime mean variations and SD of foF2, foF1, foEs, foE, h'F2, h'F, h'Es and h'E during 25-28 September 2011 for Chilton and Juliusruh Stations. The storm during this interval (on 26 September) is well developed (with Dst up to -101 nT) and larger than the 17 September event. The result of this analysis show a slight increase of foF2 and foF1 but a decrease in foEs and foE for Chilton station. The height of the F2 (h'F2) decreased (by 6.90 km) while those of the F, Es and E increased on the storm day, 26 September. Near the DHO transmitter (Juliusruh station) there is an anti-correlated variation in

480 the critical frequencies of the E and F regions; a depression of the foF2 and foF1, but increase in foEs and foE (when compared with the scenario at Chilton station). The height of the F2, F and E regions increased by 47.89 km, 16.08 km and 9.14 km, respectively (which are so far the largest increase of the parameters), while the height of the Es region decreased by 0.16 km (see, Table 5).

485   Figure 12 show the daytime mean variation and SD of foF2, foF1, foEs, foE, h'F2, h'F, h'Es and h'E during 29 October - 02 November 2011 for Chilton and Juliusruh Stations. This interval is of interest because of the fluctuation in geophysical parameters during the days preceding the storm. We include this interval to investigate the couple effect of this extended period of (30-31 Oct.) of geomagnetic disturbances preceding the storm on 1 November. It appears that energy began building up in the magnetosphere-ionosphere system after the first significant spike in V_{sw} around 7:00 am on 29th (and subsequent increase

490 on 30 Oct.) and PD around 10:00 am on 30 October until around 10:00 am on 1 November when the storm was triggered following sudden increased in V_{sw} and southward turning of the B_z (Nwankwo et al. 2021). Here, we compare the parameters' level on the relatively quiet day (29 Oct.) with those of the storm day (on 1 Nov.), since the two days preceding the storm were signicantly disturbed. The result show significant increase of foF2 and foF1 at Chilton station. Like the 17 September storm scenario, values of foEs decreased, while the foE remained unaffected for this station. The h'F2 decreased, while the h'F, h'Es

495 and h'E showed significant increase. At Juliusruh station only the critical frequency of the F2 region increase, while those of the F1, Es and E decreased. However, the increase and/or fluctuation of the parameters were significant (in most cases) during the disturbed days (30 and 31 Oct.) preceding the storm, suggesting responses of the E and F ionosphere regions (coupled to the D region) before the storm commencement (as a result of increased geomagnetic activity on the days). We present summary
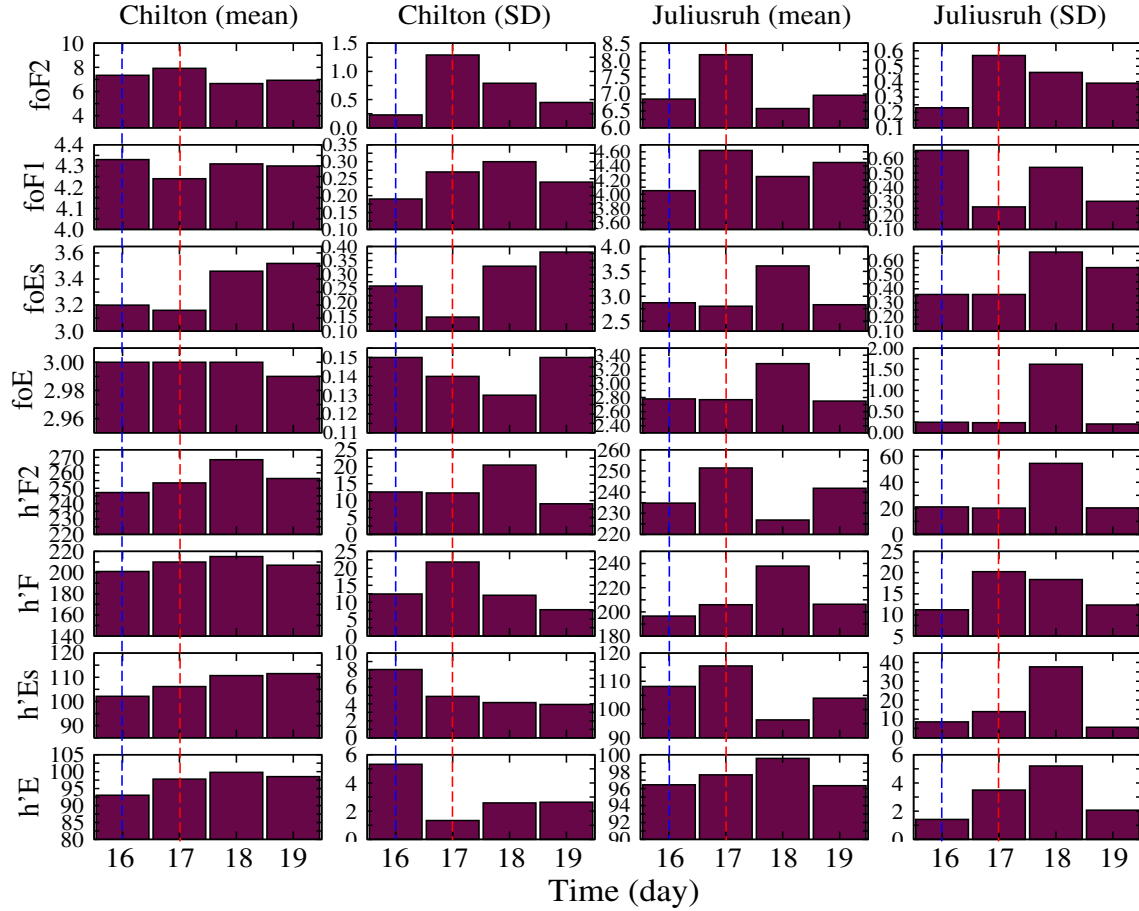
Figure 10. Daytime mean variations and standard deviation (SD) of foF2, foF1, foEs, foE, h'F2, h'F, h'Es and h'E during 16-17 September 2011 for Chilton and Juliusruh Stations. The blue broken line represent the pre-storm day values, while the red broken line represent the storm day values of the ionospheric parameters.
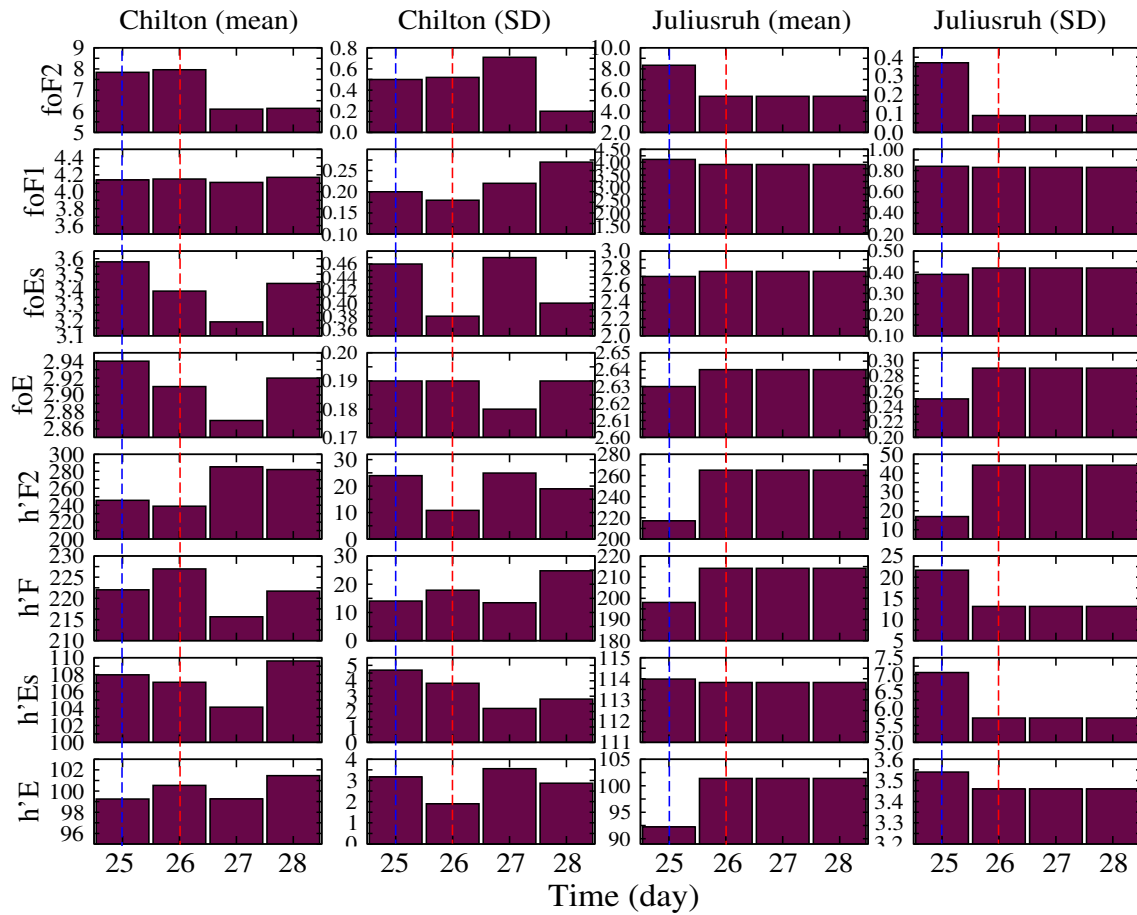
Figure 11. Daytime mean variation and SD of foF2, foF1, foEs, foE, h'F2, h'F, h'Es and h'E during 25-28 September 2011 for Chilton and Juliusruh Stations

of the storms day variations in h'F2, h'F, h'Es and h'E for the two stations in Table 5.

500

In summary, foF2, foF1, h'F2, h'F, h'Es and h'E generally showed significant increase and/or fluctuation near both transmitters (GQD and DHO) during the geomagnetic storms, whereas foEs and foE either increased (slightly) or unaffected. It appears that the observed storm-induced increase and fluctuation are largely sustained or further enhanced on the day (or days) following the event (post storm day), suggesting a continuous driving of the ionosphere by the storms and/or a substorm ef-

505 fect. Although the analysis for 1 November storm scenario showed weak correlation, variations of the parameters reflected the coupled responses of the ionosphere to energy build-up ahead of storm commencement. Nwankwo and Chakrabarti (2018) reported significant depression and fluctuations of foF2 following significant geomagnetic disturbances and/or storms in high- and mid-latitude, and distortion in the quasi-periodic pattern of the parameter. Their inference was, however, based on a prelim-
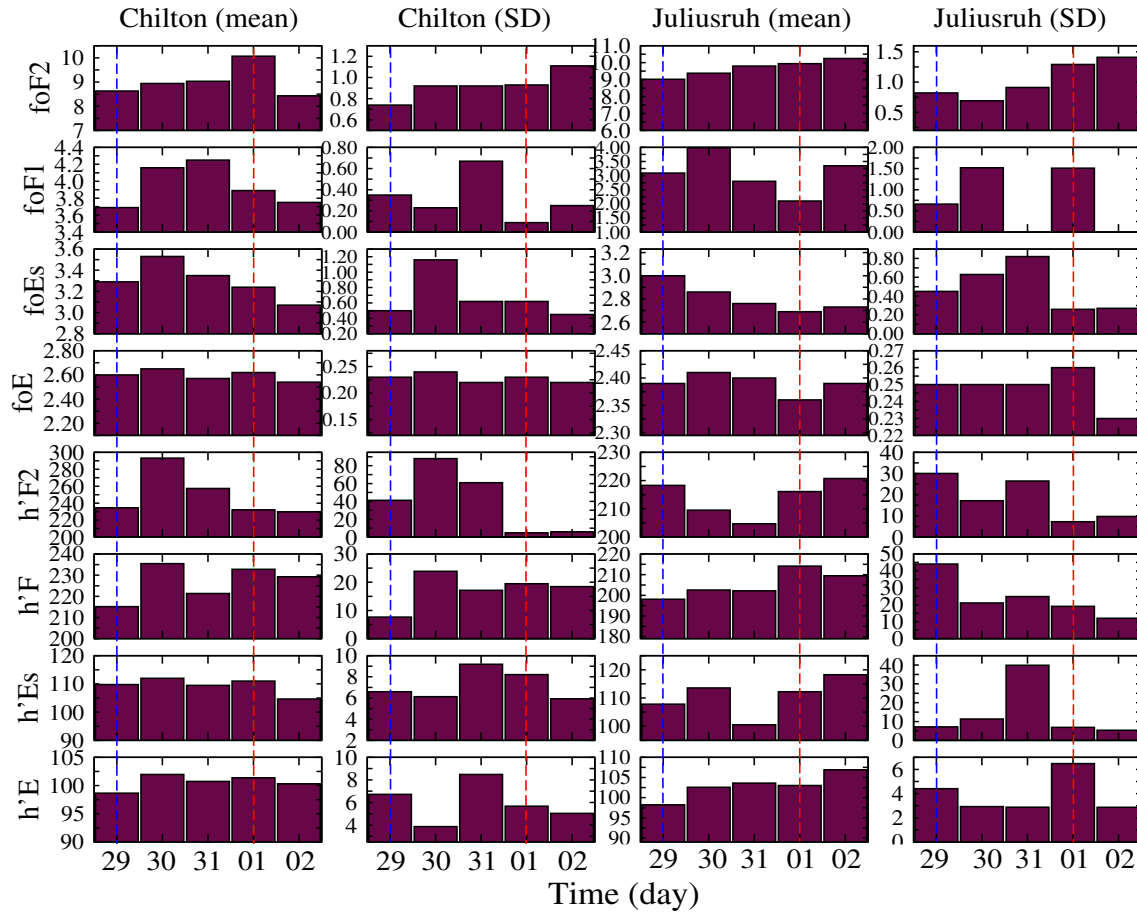
Figure 12. Daytime mean variation and SD of foF2, foF1, foEs, foE, h'F2, h'F, h'Es and h'E during 29 October - 02 November 2011 for Chilton and Juliusruh Stations.

inary analysis from the result of single ionosode station. From this comparatively detailed analysis, it is clear that the reported depression of foF2 may occur during some (isolated) storms and locations, and should, therefore, not be treated as global response. Negative storm effects (in which foF2 assumes a negative values) has also been reported (e.g., (Blanch et al., 2013; Kane, 2005)). In this analysis, the largest increase of the h'F2, h'F, h'Es and h'E occured in Juluisruh, near the DHO transmitter (see Table 5). The ionosonde observation show that fluctuations in the reference heights appear to be the dominant responses of the E and F regions to geomagnetic storms, whereas dipping of the VLF radio waves reflects storm-induced dynamics in the ionospheric D region. This observation is instructive in that the observed large ionosode increase and the large amplitude decreases in the DHO-A118 propagation path signal may be related to coupled effects between the ionospheric regions, but also suggestive of strong storm responses (more intense) around/near the DHO receiver or DHO-A118 propagation path. This result is in agreement with the recent findings reported in Nwankwo et al. (2021). Their study combined observed VLF am-

plitude variations with TEC/VTEC data obtained from multiple GNSS stations including Euskirchen in Germany (EUSK), Hailsham in UK (HERT), Paris in France (OPMT) and Naut Aran in Spain (ESCO), to investigate ionospheric response to storms over some signal propagation paths during the same events. They showed and reported simultaneous increase of VLF amplitude and enhancement of electron density profiles near the DHO transmitter. In figure 13 we show the daytime variation in VLF amplitude (red line plot) for DHO-A118 propagation path, together with VTEC values obtained from HERT (black line), EUSK (blue line), OPMT (green line) and ESCO (brown line) stations across some locations in Europe during 16-19 and 25-28 September, 24-27 October and 29 October-1 November 2011. HERT is closest to the GQD transmitter (about 508.12 km), EUSK is closest to the DHO transmitter (about 279.99 km), while ESCO is the nearest to the Receiver (about 90.47 km).

Table 5. Observed increase (or decrease) of the h'F2, h'F, h'Es and h'E during the storms on 17 and 25 September and 1 November 2011

Parameter	17 Sept. storm		26 Sept. storm		1 Nov. storm	
	Chilton	Juliusruh	Chilton	Juluisruh	Chilton	Juliusruh
h'F2	6.46 km	16.57 km	-6.90 km	47.89 km	-2.00 km	-2.18 km
h'F	8.92 km	9.42 km	4.92 km	16.08 km	17.65 km	16.04 km
h'Es	4.04 km	7.25 km	-0.88 km	-0.16 km	1.25 km	4.41 km
h'E	4.78 km	1.18 km	1.29 km	9.14 km	2.71 km	4.82 km

One can clearly observed (from fig 13) the strong dipping (or reduction) of the daytime VLF amplitude and the simultaneous increase in VTEC values on the storm days in DHO-A118 propagation path. We note the large increase of VTEC values for ESCO station located near the Receiver, especially during 17 September and 25 October storms. This feature is in agreement with the findings of (Choudhury et al., 2015), who reported that the receiver position electron density is the main factor influencing VLF signal at ionospheric sunrise time during long-duration geomagnetic storms. It is also worth noting that the ancillary information of the timing, classification and location of associated solar flares, CMEs, SPEs, and the timings for the SSCs showed that the strong storm intervals during which large dipping or decrease in DHO signal level occured were associated with SPEs (see, Table 5 in (Nwankwo et al., 2021)). The results of this effort that combined the diagnostics of the D, E and F regions (to probe geo-storm effects in the lower ionosphere) demonstrates that despite the tenuousness of the coupling between the dayside upper and lower ionospheric regions the adjoining regions of E and F plays significant role in driving the storm-induced dynamics of the D region and the associated observed responses of VLF radio waves within context of solar-terrestrial coupling arena.

4 Conclusions

In this work, we performed a diagnostic study of geomagnetic storm-induced disturbances that are coupled to the lower iono-sphere in mid-latitude D-region using propagation characteristics of VLF radio signals. We characterised the diurnal signal into five metrics (i.e MBSR, MDP, MASS, SRT and SST), and monitored the trend in variations of the signal metrics for up
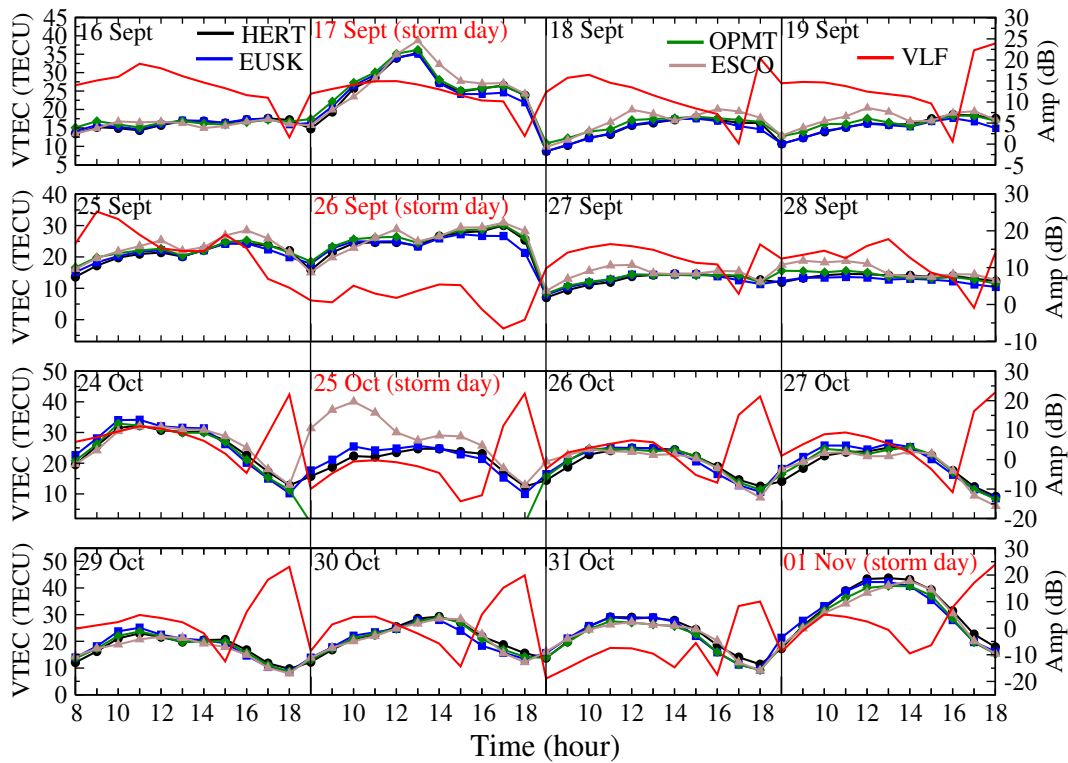
Figure 13. Daytime variation in VLF amplitude (red line plot) for DHO-A118 propagation path, together with VTEC values obtained from HERT (black line), EUSK (blue line), OPMT (green line) and ESCO (brown line) stations across some locations in Europe during 16-19 and 25-28 September, 24-27 October and 29 October-1 November 2011 (from (Nwankwo et al., 2021)).

to 20 storms between September 2011 and October 2012. The goal of the analysis is to understand deviations in the signal that are attributable to the storms. Up to five (5) storms and their effects on the signals were studied in detail, followed by statistical analysis of 15 other cases. Our results showed that the MDP exhibited characteristic dipping in about 67% and 80% of the cases in GQD-A118 and DHO-A118 propagation paths, respectively. The MBSR showed respective dipping of about 77% and 60%, while the MASS dipped by 58% and 67%. Conversely, the SRT and SST showed respective dipping of 25% and 33%, and 42% and 47%, favouring rise of the signals following storms. The MDP consistently showed strong responses to the storms that ohter metrics (followed by the MBSR and the MASS). Among other possible reasons outlined in this paper, we speculate that the responses are related to positive storm effects, the attenuation of the VLF radio waves. Of the two propagation paths examined in this study, we observed stronger dipping of the VLF amplitude of DHO-A118 propagation path during the storms. To understand the state of the ionosphere over the propagation paths and how it affects the VLF responses, we further analysed virtual heights (h'E, h'F1 and h'F2) and critical frequencies (foE, foF1, and foF2) of the E and F regions (from ionosonde stations near the GQD and DHO transmitters). The results of this analysis showed a significant increase and/or fluctuation in the height of the E and F regions (h'F2, h'F, h'Es and h'E) near both transmitters during the geomagnetic storms,

with the largest increase occurring in Juluisruh (Germany) station, near the DHO transmitter. This scenario suggest a strong storm responses over the region, possibly leading to the large dipping of VLF amplitude for DHO-A118 propagation path. The ionosonde observation show that fluctuations in the reference heights appear to be the dominant responses of the E and F
560   regions to geomagnetic storms, whereas dipping of the VLF radio waves reflects storm-induced dynamics in the ionospheric D region. Our findings demonstrates that ionospheric E and F regions plays significant role in driving the storm-induced dynamics of the D region and the associated observed responses of VLF radio waves (within context of solar-terrestrial coupling arena) despite the tenuousness of the coupling between the dayside upper and lower ionospheric regions.

Competing interests.   The authors declare that they have no conflict of interest

565   *Acknowledgements.* V.U.J. Nwankwo acknowledge the World Academy of Science (TWAS), Trieste, Italy and the S.N. Bose National Centre for Basics Sciences (SNBNCBS) for the awarde of Postgraduate research fellowship during which a portion of this work was done. The authors thank Dr. Bruce Tsurutani (Jet Propulsion Laboratory, California Institute of Technology) and Dr. Jan Lastovicka for clarification of some aspects of geomagnetic data and processes. We also acknowledge the UK Solar System Data Centre (UKSSDC) for ionosonde data and also thank Matthew Wild for assisting with ionosode data acquisition when it was difficult to proceed.

References

Abd Rashid, M. M., Ismail, M., Hasbie, A. M., Salut, M. M., & Abdullah, M. (2013, July). VLF observation of D-region disturbances associated with solar flares at UKM Selangor Malaysia. In 2013 IEEE International Conference on Space Science and Communication (IconSpace) (pp. 249-252). IEEE.

Ahrens C.D. and R. Henson (2021), Meteorology Today: An Introduction to Weather, Climate and the Environment, 736 p., ISBN-13: 978-0357452073, Cengage Learning, Boston, MA.

Akasofu, S. (2020), Relationship Between Geomagnetic Storms and Auroral/Magnetospheric Substorms: Early Studies, Frontiers Astron. Space Sci, 7, 16 p. doi: 10.3389/fspas.2020.604755

Akasofu S.-I. (2018), A Review of the Current Understanding in the Study of Geomagnetic Storms, Int. J. Earth Sci. Geophys., 4, 1, 13 p. doi: 10.35840/2631-5033/1818

Akasofu S.-I. (1964), The development of the auroral substorm, Planet. Space Sci., 12, 4, pp. 273-282. doi: https://doi.org/10.1016/0032-0633(64)90151-5

Alfonsi L., Andrew J. Kavanagh, Ermanno Amata et al. (2008), Probing the high latitude ionosphere from ground-based observations: The state of current knowledge and capabilities during IPY (2007-2009), J Atm. Solar-Terres. Phys., 70, 2293 - 2308.

Andersson M.E., P.T. Verronen, D.R. Marsh, S.-M. Paivarinta and J.M.C. Plane (2016), WACCM-D—Improved modeling of nitric acid and active chlorine during energetic particle precipitation, J. Geophys. Res. Atmos., 121, 17, pp. 10328–10341. doi:10.1002/2015JD024173

Angelopoulos V., A. Artemyev, T.D. Phan and Y. Miyashita (2020), Near-Earth Magnetotail Reconnection Powers Space Storms, Nat. Phys. 2020, 25 p. doi: 10.1038/s41567-019-0749-4

Appleton E.V. (1927) The Existence of more than one Ionised Layer in the Upper Atmosphere, Nature 120, 330, 1476-4687, https://doi.org/10.1038/120330a0

Appleton, E.V. (1933), Meeting for discussion on the ionosphere, Proc. R. Soc. Lond. A, 141, 845, pp. 697-721, doi: https://doi.org/10.1098/rspa.1933.0149.

Appleton E. and M. Barnett (1925a), Local Reflection of Wireless Waves from the Upper Atmosphere, Nature, 115, pp. 333-334. doi:https://doi.org/10.1038/115333a0.

Appleton E.V. and M.A.F. Barnett (1925b), On some direct evidence for downward atmospheric reflection of electric rays, Proc. R. Soc. Lond. A., 109, 752, pp. 621-641, doi: http://doi.org/10.1098/rspa.1925.0149

Appleton E.V. and M.A.F. Barnett (1926), On wireless interference phenomena between ground waves and waves deviated by the upper atmosphere, Proc. R. Soc. Lond. A, 113, 764, pp.450-458. doi: http://doi.org/10.1098/rspa.1926.0164.

Appleton E.V. and R. Naismith (1935), Some further measurements of upper atmospheric ionization, Proc. R. Soc. Lond. A, 150, 871, pp. 685-708 doi: http://doi.org/10.1098/rspa.1935.0129

Araki T. (1974), Anomalous Phase Changes of Trans equatorial VLF Radio Waves during Geomagnetic Storms, J Geophys. Res., 79, 4811-4813

Aryan H., J. Bortnik, N.P. Meredith, R.B. Horne, D.G. Sibeck and M.A. Balikhin (2021), Multi-parameter chorus and plasmaspheric hiss wave models, J. Geophys. Res.: Space Phys., 126, e2020JA028403, 14 p. doi: https://doi.org/10.1029/2020JA028403

Aubry M.P., C.T. Russell and M.G. Kivelson (1970), Inward motion of the magnetopause before a substorm, J. Geophys. Res., 75, 34, pp. 7018-7031. doi: 10.1029/JA075i034p07018

Baker D. N. (2000), Effects of the Sun on the Earth's environment, J. Atm. Solar-Terres. Phys., 62, 1669-1681.

Banks P.M. and Kockarts G. (1973), Aeronomy, Academic Press Inc, NY, USA

Baker D.N., V. Hoxie, H. Zhao, A.N. Jaynes, S. Kanekal, X. Li and S. Elkington (2019), Multiyear measurements of radiation belt electrons: Acceleration, transport, and loss, J. Geophys. Res.: Space Phys., 124, 4, pp. 2588–2602. doi: https://doi.org/10.1029/2018JA026259

610   Bates D.R. and H.S.W. Massey (1946), The basic reactions in the upper atmosphere, Proc. R. Soc. Lond. A., 187, 1010, pp. 261-296. doi: http://doi.org/10.1098/rspa.1946.0078

Bates D.R. and H.S.W. Massey (1947), The basic reactions in the upper atmosphere II. The theory of recombination in the ionized layers, Proc. R. Soc. Lond. A, 192, 1028, pp. 1-16. doi: http://doi.org/10.1098/rspa.1947.0134

Barr R., D.L. Jones and C.J. Rodger (2000), ELF and VLF radio waves, J. Atmos. Solar Terr. Phys., 62, 1, pp. 1689-1718, doi: https://doi.org/10.1016/S1364-6826(00)00121-8.

615   Belrose J.S. and L. Thomas (1968), Ionization changes in the middle latitude D-region associated with geomagnetic storms, J. Atmos. Sol. Terr. Phys., 30, pp. 1397-1413. doi: 10.1016/S0021-9169(68)91260-9

Bennington, T.W. (1944), Radio Waves and the Ionosphere, Nature, 154, p. 413. doi: https://doi.org/10.1038/154413a0

Benson R.F. (2010), Four Decades of Space-Borne Radio Sounding, Radio Science Bulletin, 333, NASA Tech. Rep. 20110011009, 21 p

620   Betz H.D., K. Schmidt and W.P. Oettinger (2009), LINET – An International VLF/LF Lightning Detection Network in Europe, in Lightning: Principles, Instruments and Applications, eds. Betz H.D., U. Schumann and P. Laroche, Springer, Dordrecht. $https://doi.org/10.1007/978-1-4020-9079-0\_5$

Beynon W.J.G. (1969) The physics of the ionosphere, Science Progress, 57 (227), pp. 415-433.

Bibl K. (1998). Evolution of the ionosonde. Annals of Geophysics, 41(5-6).

625   Bilitza, D. (1990), International Reference Ionosphere 1990, NSSDC, Report 90-22, Greenbelt, MD, 160 p. Available at "https://ntrs.nasa.gov/api/citations/19910021307/downloads/19910021307.pdf", Last accessed: 02 December 2021

Bilitza D. (2001), International Reference Ionosphere 2000, Radio Sci., 36, 2, pp. 261–275 doi: https://doi.org/10.1029/2000RS002432.

Bilitza D. (2018), IRI the International Standard for the Ionosphere, Adv. Radio Sci., 16, pp. 1–11, https://doi.org/10.5194/ars-16-1-2018

Bilitza D. and B.W. Reinisch (2008), International Reference Ionosphere 2007: Improvements and new parameters, Adv. Space Res., 42,
630   pp.599–609. doi: https://doi.org/10.1016/j.asr.2007.07.048

Bilitza D. (1998), The E- and D-region in IRI, Adv. Space Res., 21, 6, pp. 871-874. doi: https://doi.org/10.1016/S0273-1177(97)00645-5

Bilitza D. (1981), Electron density in the D-region as given by the International Reference Ionosphere, in "International Reference Ionosphere IRI 79", UAG-82, World Data Center A for Solar-Terrestrial Physics, eds. Lincoln, J.V. and R.O. Conkright, pp. 7-10. Available at "$https://www.ngdc.noaa.gov/stp/space-weather/online-publications/stp\_uag/$", Last accessed: 02 December 2021

635   Blanc M. (1988), Magnetosphere-Ionosphere Coupling, Computer Physics Communications, 49, 1, pp. 103-118. doi: https://doi.org/10.1016/0010-4655(88)90219-6

Blake J.B., U.S. Inan, M. Walt, T.F. Bell, J. Bortnik, D.L. Chenette and H.J. Christian (2001), Lightning-induced energetic electron flux enhancements in the drift loss cone, J. Geophys. Res., 106, A12, pp. 29733–29744. doi: 10.1029/2001JA000067

Blanc M. and A. Richmond (1980), The ionospheric disturbance dynamo, J. Geophys. Res., 85, A4, pp. 1669-1686. doi:
640   10.1029/JA085iA04p01669

Blanch, E., S. Marsal, A. Segarra, J.M. Torta, D. Altadill, and J.J. Curto (2013), Space weather effects on Earth's environment associated to the 24-25 October 2011 geomagnetic storm, Space Weather, 11, 153-168, doi:10.1002/swe.20035.

Borovsky J. E. and Denton M. H. (2006), Differences between CME-driven storms and CIR-driven storms, J Geophys. Res., 111

645 Bonde R.E.F., R.E. Lopez and J.Y. Wang (2018), The effect of IMF fluctuations on the subsolar magnetopause position: A study using a global MHD model, J. Geophys. Res.: Space Phys., 123, 4, pp. 2598–2604. https://doi.org/10.1002/2018JA025203

Borovsky J.E. and Y.Y. Shprits (2017), Is the Dst index sufficient to define all geospace storms? J. Geophys. Res.: Space Phys., 122, pp. 11543 - 11547. doi: https://doi.org/10.1002/2017JA024679

Bucha V. and Bucha Jr. V., Geomagnetic forcing of changes in climate and in the atmospheric circulation, J. Atmos. Sol-Terr. Phys., 60, 145 - 169.

650 Budden K.D. (1951) I. The Propagation of a Radio-Atmospheric, The London, Edinburgh, and Dublin Philosophical Magazine and Journal of Science, 42, 324, pp. 1-19. doi: 10.1080/14786445108561218.

Budden K.G. (1953), The propagation of very low frequency radio waves to great distances, Philosophical Magazine, 44, 352, pp. 504-513, doi: https://doi.org/10.1080/14786440508520335.

Budden K.G. (1957), "The "Waveguide Mode" Theory of the Propagation of Very-Low-Frequency Radio Waves," in Proc. IRE, 45, 6, pp. 655 772-774. doi: 10.1109/JRPROC.1957.278471

Breit G., and Tuve, M. A. (1925). A radio method of estimating the height of the conducting layer. Nature, 116(2914), 357-357.

Buonsanto M.J. (1999), Ionospheric storms: a review, Space Sci. Rev., 88, 563 - 601.

Buresova D. and Lastovicka J. (2007), Pre-storm enhancements of foF2 above Europe, Adv. Space Res. 39, 1298-1303.

Burch J.L. (2016), Magnetosphere-Ionosphere Coupling, Past to Future, in Magnetosphere-Ionosphere Coupling in the Solar System, Geo- 660 physical Monograph Series, eds. Chappell, C.R., R.W. Schunk, P.M. Banks, J.L. Burch and R.M. Thorne, ISBN:9781119066774, pp. 1-17, doi: https://doi.org/10.1002/9781119066880.ch1

Burke W. J. (2000), Magnetosphere-ionosphere coupling: selected topics, J Atmo. Solar-Terres. Phys., 62, 817-824.

Burns A. G., S.C. Solomon, L. Qian, W. Wang, B.A. Emery, M. Wiltberger, and D.R. Weimer (2012), The effects of Corotating interaction region/High speed stream storms on the thermosphere and ionosphere during the last solar minimum, J Atm. Solar-Terres Phys., 83, 79-87

665 Cassak P.A. (2016), Inside the Black Box: Magnetic Reconnection and the Magnetospheric Multiscale Mission, Space Weather, 14, pp. 186-197. doi: 10.1002/2015SW001313

Chakrabarti S.K., S. Sasma and S. Chakrabart (2010), Ionospheric anomaly due to seismic activities – Part 2: Evidence from D-layer prepa- ration and disappearance times, Nat. Hazards Earth Syst. Sci., 10, 1751–1757, 2010., doi: https://doi.org/10.5194/nhess-10-1751-2010

Chakraborty M., S. Kumar, B.K. De and A. Guha (2015), Effects of geomagnetic storm on low latitude ionospheric total electron content: A 670 case study from Indian sector, J. Earth Syst. Sci., 124, pp. 1115–1126. doi: https://doi.org/10.1007/s12040-015-0588-3

Chandra R., N. Gopalswamy, P. Mäkelä, H. Xie, S. Yashiro, S. Akiyama, W. Uddin, A.K. Srivastava, N.C. Joshi, R. Jain, A.K. Awasthi, P.K. Manoharan, K. Mahalakshmi, V.C. Dwivedi, D.P. Choudhary and N.V. Nitta (2013), Solar energetic particle events during the rise phases of solar cycles 23 and 24, Adv. Space Res., 52, 12, pp. 2102-2111. doi: https://doi.org/10.1016/j.asr.2013.09.006

Chapman, S. and V. Ferraro (1930), A New Theory of Magnetic Storms, Nature, 126, pp. 129–130. https://doi.org/10.1038/126129a0

675 Chapman S. (1931), The absorption and dissociative or ionizing effect of monochromatic radiation in an atmosphere on a rotating earth, Proc. Phys. Soc., 43, 26, pp. 26-45. doi: doi:10.1088/0959-5309/43/1/305

Chapman J.H. and E.S. Warren (1968), Topside sounding of the Earth's ionosphere, Space Sci. Rev.,8, 5-6, pp. 846-865. doi: 10.1007/BF00175119

Chenette D.L., Datlowe D. W., Robinson R. M., Schumaker T. L., Vondrak R. R., and Winningham J. D. (1993), Atmospheric energy input 680 and ionization by energetic electrons during the geomagnetic storm of 8-9 November 1991, Geophys. Res. Lett., 20, 1323.

Chilton C.J., D.D. Crombie and A.G. Jean (1964), Phase Variations in V.L.F. Propagation (Chapter 19), in "Propagation of Radio Waves at Frequencies Below 300 kc/s: Proceedings of the Seventh meeting of the AGARD Ionospheric Research Committee, Munich 1962", ed. W.T. Blackband, AGARDograph, Volume 74, pp. 257-290, Elsevier, Amsterdam, Netherlands. doi: https://doi.org/10.1016/B978-0-08-010268-9.50023-8

Choi, Y., Y.-J. Moon, S. Choi, J.-H. Baek, S.S. Kim, K,-S. Cho and G.S. Choe (2009), Statistical Analysis of the Relationships among Coronal Holes, Corotating Interaction Regions, and Geomagnetic Storms, Sol. Phys., 254, pp. 311–323. doi: https://doi.org/10.1007/s11207-008-9296-3

Choudhury A., B.K. De, A. Guha and R. Roy (2015), Long-duration geomagnetic storm effects on the D region of the ionosphere: Some case studies using VLF signal, J. Geophys. Res. Space Physics, 120, pp. 778– 787. doi:10.1002/2014JA020738.

Chuo, Y. J., C. C. Lee, W. S. Chen, and B. W. Reinisch (2013), Comparison of the characteristics of ionospheric parameters obtained from FORMOSAT-3 and digisonde over Ascension Island, Ann. Geophys., 31, 787-794.

Clilverd M. A., Rodger C. J., Gamble R. J., Ulich T., Raita T., Seppala A., Green J. C., Thomson N. R., Sauvaud J. A., and Parrot M. (2010), Ground-based estimates of outer radiation belt energetic electron precipitation fluxes into the atmosphere, J Geophys. Res., 115, A12304.

Clilverd M.A., C.J. Rodger, J.J. Neal and K. Cresswell-Moorcock (2014), "Remote sensing space weather events through ionospheric radio: The AARDDVARK network," 2014 XXXIth URSI General Assembly and Scientific Symposium (URSI GASS), pp. 1-1, doi: 10.1109/UR-SIGASS.2014.6929921

Clilverd M.A., C.J. Rodger, N.R. Thomson, J.B. Brundell, T. Ulich, J. Lichtenberger, N. Cobbett, A.B. Collier, F.W. Menk, A. Seppälä, P.T. Verronen and E. Turunen (2009), Remote sensing space weather events: Antarctic-Arctic Radiation-belt (Dynamic) Deposition-VLF Atmospheric Research Konsortium network, Space Weather, 7, 4, S04001. doi: 10.1029/2008SW000412

Clilverd M.A., A. Seppala, C.J. Rodger, N.R. Thomson, J. Lichtenberger and P. Steinbach (2007), Temporal variability of the descent of high-altitude NOX inferred from ionospheric data, J. Geophys. Res.: Space Physics, 112, A9, A09307, 10 p. doi: 10.1029/2006JA012085

Colwell R. and A. Friend (1936), The D Region of the Ionosphere, Nature 137, p. 782. https://doi.org/10.1038/137782a0

Cowley S. W. H., Davies J. A., Grocott A., Khan H., Lester M., McWilliams K. A., Milan S. E., Provan B., Sandholt P. E., Wild J. A. and Yeoman T. K. (2003), Solar-wind-magnetosphere-ionosphere interactions in the Earth's plasma environment, Phil. Trans. R. Soc. Lond. A, 361, 113-126.

Crombie D.D. (1964), Phase and Time Variations in VLF Propagation Over Long Distances, J. Res. NBS: Radio Science, 68D, 11, pp. 1223-124.

Crombie D.D. (1966), Further Observations of Sunrise and Sunset Fading of Very-Low-Frequency Signals, Radio Science, 1, doi: 10.1002/rds19661147

Cummer S. A., Inan, U. S., & Bell, T. F. (1998). Ionospheric D region remote sensing using VLF radio atmospherics. Radio Science, 33(6), 1781-1792.

Danilov A. D. and Lastovicka J. (2001), Effects of Geomagnetic Storms on the Ionosphere and Atmosphere, Inter. J. Geomagn. Aeron., 2, 209-224.

Danilov, A.D. and N.V. Smirnova (1995), Improving the 75 to 300 km ion composition model of the IRI, Adv. Space Res., 15, 2, pp. 171-177. doi: https://doi.org/10.1016/S0273-1177(99)80044-1.

Davies K. and G.K. Hartmann (1997), Studying the ionosphere with the Global Positioning System, Radio Sci., 32, 4, pp. 1695-1703, doi:10.1029/97RS00451

Dellinger J. H. (1937), Sudden ionospheric disturbances, Terr. Magn. Atmos. Electr., 42, 1, pp. 49-53, doi: 10.1029/TE042i001p00049.

Dickinson P.H.G. and F.D.G Bennett (1978), Diurnal variations in the D-region during a storm after-effect, J. Atmos. Terr. Phys., 40, 5, pp. 549-558. doi: https://doi.org/10.1016/0021-9169(78)90092-2

Dierckxsens M., K. Tziotziou, S. Dalla, I. Patsou, M.S. Marsh, N.B. Crosby, O. Malandraki and G. Tsiropoula (2015), Relationship between Solar Energetic Particles and Properties of Flares and CMEs: Statistical Analysis of Solar Cycle 23 Events, Sol. Phys., 290, 3, pp. 841-874. doi: 10.1007/s11207-014-0641-4

Dougherty J.P. and D.T. Farley (1961), A theory of incoherent scattering of radio waves by a plasma, Proc. R. Soc. Lond. A, 259, 1296, pp. 79–99. doi: http://doi.org/10.1098/rspa.1960.0212

Dougherty J.P., and D.T. Farley (1963), A theory of incoherent scattering of radio waves by a plasma: 3. Scattering in a partly ionized gas, J. Geophys. Res., 68, 19, pp 5473–5486. doi:10.1029/JZ068i019p05473

Dungey J.W. (1961), Interplanetary Magnetic Field and the Auroral Zones, Phys. Rev. Lett. 6, 47.

Eccles J.V., R.D. Hunsucker, D. Rice and J.J. Sojka (2005), Space weather effects on midlatitude HF propagation paths: Observations and a data-driven D region model, Space Weather, 3, S01002, xx p. doi: 10.1029/2004SW000094

Evans J.V. (1969a), Millstone Hill Thomson scatter results for 1965, Tech. Rep. 474, Lincoln Lab., Mass. Inst. of Technol., Cambridge, 8 Dec. doi: http://hdl.handle.net/1721.1/97666

Evans J.V. (1969b), Theory and practice of ionosphere study by Thomson scatter radar, in Proc. IEEE, 57, 4, pp. 496-530. doi: 10.1109/PROC.1969.7005.

Fagundes P. R., Cardoso, F. A., Fejer, B. G., Venkatesh, K., Ribeiro, B. A. G., & Pillat, V. G. (2016). Positive and negative GPS-TEC ionospheric storm effects during the extreme space weather event of March 2015 over the Brazilian sector. Journal of Geophysical Research: Space Physics, 121(6), 5613-5625.

Friedrich, M. and K.M. Torkar (1992), An empirical model of the non-auroral D Region, Radio Sci., 27, 6, pp. 945-953. doi:10.1029/92RS01929

Fairfield D.H. (1971), Average and unusual locations of the Earth's magnetopause and bow shock, J. Geophys. Res., 76, 28, pp. 6700-6716, doi:10.1029/JA076i028p06700

Farley D.T., J.P. Dougherty and D.W. Barron (1961), A Theory of Incoherent Scattering of Radio Waves by a Plasma II. Scattering in a Magnetic Field, Proc. Royal Soc. London A, 263, 1313, pp. 238-258. doi: https://www.jstor.org/stable/2414112

Fejer B.G., M.F. Larsen and D.T. Farley (1983), Equatorial disturbance dynamo electric fields, Geophys. Res. Lett., 10, 7, pp. 537-540. https://doi.org/10.1029/GL010i007p00537

Forbush S.E. (1954), World-wide cosmic ray variations, 1937–1952, J. Geophys. Res., 59, 4, pp. 525– 542, doi: 10.1029/JZ059i004p00525

Fuller-Rowell T.J., M.V. Codrescu, R.J. Moffett and S. Quegan (1994), Response of the thermosphere and ionosphere to geomagnetic storms, J. Geophys. Res., 99, A3, pp. 3893-3914. doi: 10.1029/93JA02015

Gardiner G.W. (1969), Origin of the Term Ionosphere, Nature, 224, p. 1096. doi: https://doi.org/10.1038/2241096a0

Gauss C.F. (1938), Allgemeine Theorie des Erdmagnetismus, in: Resultate aus den Beobachtungen des magnetischen Vereins im Jahre 1838, edited by: Gauss, C.F. and W. Weber, pp. 1–57, Weidmannsche Buchhandlung, Leipzig.

Ganushkina N.Y., M.W. Liemohn and S. Dubyagin (2018), Current systems in the Earth's magnetosphere, Reviews of Geophysics, 56, 2, pp. 309-332. https://doi.org/10.1002/2017RG000590

George H., E. Kilpua, A. Osmane, T. Asikainen, Milla M. H. Kalliokoski1, C.J. Rodger, S. Dubyagin and M. Palmroth (2020), Outer Van Allen belt trapped and precipitating electron flux responses to two interplanetary magnetic clouds of opposite polarity, Ann. Geophys., 38, 4, pp. 931–951. doi: https://doi.org/10.5194/angeo-38-931-2020

Glassmeier K.-H. and B.T. Tsurutani (2014), Carl Friedrich Gauss - General Theory of Terrestrial Magnetism - a revised translation of the German text, Hist. Geo Space. Sci., 5, pp. 11–62. doi: https://doi.org/10.5194/hgss-5-11-2014

Gonzalez, W. D., Joselyn, J. A., Kamide, Y., Kroehl, H. W., Rostoker, G., Tsurutani, B. T., and Vasyliunas, V. M. (1994). What is a geomagnetic storm?. Journal of Geophysical Research: Space Physics, 99(A4), 5771-5792.

Gonzalez W.D., B.T.Tsurutani and A.L. Clúa de Gonzalez (1999), Interplanetary origin of geomagnetic storms, Space Sci. Rev., 88, pp. 529-562. doi: https://doi.org/10.1023/A:1005160129098

Gopalswamy N. (2018), Chapter 2 - Extreme Solar Eruptions and their Space Weather Consequences, in "Extreme Events in Geospace", pp. 37-63, ed. Buzulukova, N., Elsevier Publishing Co., Amsterdam, Netherlands. doi: https://doi.org/10.1016/B978-0-12-812700-1.00002-9

Gosling J.T. and Pizzo V.J. (1999), Formation and evolution of corotating interaction regions and their three dimensional structure, Space Sci. Rev. 89, 2152.

Grafe, A., E.-A. Lauter, B. Nikutowski and C.-U. Wagner (1980), Precipitation of Energetic Electrons into the Mid-Latitude Ionosphere After Geomagnetic Storms, ed: Rycroft, M.J., COSPAR Colloquia Series, 20, pp. 157-162, Pergamon, Oxford, U.K. doi: https://doi.org/10.1016/S0964-2749(13)60035-9

Greenwald R. A., Baker, K. B., Dudeney, J. R., Pinnock, M., Jones, T. B., Thomas, E. C., ... & Yamagishi, H. (1995). Darn/superdarn. Space Science Reviews, 71(1), 761-796.

Greenwald R.A. (2021), History of the Super Dual Auroral Radar Network (SuperDARN)-I: pre-SuperDARN developments in high frequency radar technology for ionospheric research and selected scientific results, Hist. Geo Space. Sci., 12, 77-93. doi: https://doi.org/10.5194/hgss-12-77-2021

Greer K. R., Immel, T., and Ridley, A. (2017), On the variation in the ionospheric response to geomagnetic storms with time of onset, J. Geophys. Res. Space Physics, 122, pp. 4512–4525, doi: 10.1002/2016JA023457

Gross N.C. and M.B. Cohen (2020), VLF remote sensing of the D region ionosphere using neural networks, J. Geophys. Res Space Phys., 125, e2019JA027135, xx p. https://doi.org/10.1029/2019JA027135

Gu T.T. and H.L. Xu (2020), Mode Interferences of VLF Waves in the Presence of an Anisotropic Terrestrial Waveguide, in Electromagnetic Propagation and Waveguides in Photonics and Microwave Engineering, ed. P. Steglich, 23 p., InTechOpen Limited, London. doi: 10.5772/intechopen.91238

Gu, X., S. Xia, S. Fu, Z. Xiang, B. Ni, J. Guo and X. Cao (2020), Dynamic Responses of Radiation Belt Electron Fluxes to Magnetic Storms and their Correlations with Magnetospheric Plasma Wave Activities, Astrophys. J., 891, 2, 127, 11 p. doi: https://doi.org/10.3847/1538-4357/ab71fc

Guerrero A., J. Palacios, M. Rodríguez-Bouza, I. Rodríguez-Bilbao, A. Aran, C. Cid, M. Herraiz, E. Saiz, G. Rodrigues-Caderot and Y. Cerrato (2017) Storm and substorm causes and effects at midlatitude location for the St. Patrick's 2013 and 2015 events, J. Geophys. Res.: Space Phys., 122, 10, pp. 9994–10,011. doi: https://doi.org/10.1002/2017JA024224

Häggström, I. (2017), The ESPAS e-infrastructure: Access to data from near-Earth space, in The ESPAS E-infrastructure, ISBN: 9782759819492, eds. Belehaki, A., M. Hapgood and J. Watermann, EDP Sciences, Les Ulis, France, pp. 117-126. doi: https://doi.org/10.1051/978-2-7598-1949-2.c012

Hajra R. (2021), September 2017 Space-Weather Events: A Study on Magnetic Reconnection and Geoeffectiveness, Sol. Phys., 296, 50, 18 p. doi: https://doi.org/10.1007/s11207-021-01803-7

Hayes, L.A., O.S.D. O'Hara, S.A. Murray, P.T. Gallagher (2021), Solar Flare Effects on the Earth's Lower Ionosphere, Solar Stellar Astrophys., submitted, doi: 10.1007/s11207-021-01898-y

795   Heaviside O. (1902) Telegraphy. InEncyclopaedia Britannica, p. 214. Edinburgh and London:Adam and Charles Black.

Heelis, R. A. and A. Maute (2020). Challenges to understanding the Earth's ionosphere and thermosphere, J. Geophys. Res.: Space Phys., 125, 7, e2019JA027497. doi: https://doi.org/10.1029/2019JA027497

Hegde, S., M.G. Bobra and P.H. Scherrer (2018), Classifying Signatures of Sudden Ionospheric Disturbances, Research Notes of the AAS, 2, 3, Article 162, doi: 10.3847/2515-5172/aade47

800   Heikkila W. (2011), Earth's Magnetosphere, Elsevier Kidlington, Oxford, UK.

Horne R.B., M.M. Lam and J.C. Green (2009), Energetic electron precipitation from the outer radiation belt during geomagnetic storms, Geophys. Res. Lett., 36, 19, L19104, doi:10.1029/2009GL040236

Hui D., D. Chakrabarty, R. Sekar, G.D. Reeves, A. Yoshikawa and K. Shiokawa (2017), Contribution of storm time substorms to the prompt electric field disturbances in the equatorial ionosphere, J. Geophys. Res. Space Physics, 122, 5, pp. 5568-5578. doi:10.1002/2016JA023754

805   Immel T.J. and A.J. Mannucci (2013), Ionospheric redistribution during geomagnetic storms, J. Geophys. Res. Space Physics, 118, pp. 7928–7939. doi: 10.1002/2013JA018919.

Inan U.S., S.A. Cummer and R.A. Marshall (2010), A survey of ELF and VLF research on lightning-ionosphere interactions and causative discharges, J. Geophys. Res., 115, A6, A00E36, doi: 10.1029/2009JA014775

Hunsucker R.D. (1992), Auroral and polar-cap ionospheric effects on radio propagation, IEEE Trans. Antennas Propagation, 40, 7, pp.

810   818-828. doi: 10.1109/8.155747

Jackson J.E. (1986), Alouette-ISIS Program Summary, NSSDC/WDC-A-R & S 86-09, 94 p.

Jordanova, V.K., R. Ilie and M.W. Chen (2020), Introduction and historical background, in Ring Current Investigations (The Quest for Space Weather Prediction), ISBN 9780128155714, eds. Jordanova, V.K., R. Ilie and M.W. Chen, pp. 1-13, Elsevier, Amsterdam. doi: https://doi.org/10.1016/B978-0-12-815571-4.00001-9.

815   Kane R.P. (2005), Ionospheric f oF2 anomalies during some intense geomagnetic storms, Ann Geophys., 23, 2487-2499.

Jackson J.E. (1986), Alouette-ISIS Program Summary, NSSDC/WDC-A-R& S 86-09, 94 p.

Johnson C.Y. (1966), Ionospheric composition and density from 90 to 1200 kilometers at solar minimum, J. Geophys. Res., 71, 1, pp. 330-332, doi:10.1029/JZ071i001p00330

Janvier M., P. Demoulin, J. Guo, S. Dasso, F. Regnault, S. Topsi-Moutesidou, C. Gutierrez and B. Perri (2021), The Two-step Forbush

820   Decrease: A Tale of Two Substructures Modulating Galactic Cosmic Rays within Coronal Mass Ejections, Astrophys. J., 922, 2, 15 p. doi: 10.3847/1538-4357/ac2b9b

Kovacs T., J.M.C. Plane, W. Feng, T. Nagy, M.P. Chipperfield, P.T. Verronen, M.E. Andersson, D.A. Newnham, M.A. Clilverd and D.R. Marsh (2016), D-region ion–neutral coupled chemistry (Sodankylä Ion Chemistry, SIC) within the Whole Atmosphere Community Climate Model (WACCM 4) – WACCM-SIC and WACCM-rSIC, Geosci. Model Dev., 9, 9, pp. 3123–3136. doi: https://doi.org/10.5194/gmd-

825   9-3123-2016

Kennelly A. (1902) On the Elevation of the Electrically-Conducting Strata of the Earth's Atmosphere. Elee. TVorld and Engr., 39, p. 473.

Kelley M. C. (1989), The Earth's Ionosphere, Academic Press Inc. San Diego, California.

Kelley M.C. (2009), The Earth's Ionosphere, Plasma Physics and Electrodynamics, 576 p., ISBN: 978012088425, Academic Press, Cambridge, Massachusetts, U.S.A.

830   Kanekal S. and Y. Miyoshi (2021), Dynamics of the terrestrial radiation belts: a review of recent results during the VarSITI (Variability of the Sun and Its Terrestrial Impact) era, 2014–2018. Prog Earth Planet Sci 8, 35, 22 p. doi: https://doi.org/10.1186/s40645-021-00413-y

Kerrache F., S.N. Amor and S. Kumar (2021), Ionospheric D region disturbances due to FAC and LEP associated with three severe geomagnetic storms as observed by VLF signals. J. Geophys. Res.: Space Phys., 126, 2, e2020JA027838, 13 p. doi: https://doi.org/10.1029/2020JA027838

835 Kikuchi T. and Evans D.S. (1983), Quantitative study of substorm-associated VLF phase anomalies and precipitating energetic electrons on November 13, 1979, J. Geophys. Res., 88, 871-880.

Kilfoyle B. and F. Jacka (1968), Geomagnetic L Coordinates, Nature, 220, pp. 773–775. doi: https://doi.org/10.1038/220773a0

Kim R.-S., K.-H. Cho, Y.-D. Kim, Y.-J Park, Y.-J Moon, Y. Yi, J. Lee, H. Wang, H. Song and M. Dryer (2008), CME Earthward Direction as an Important Geoeffectiveness Indicator, Astrophys. J., 677, 2, pp. 1378-1384. doi: 10.1086/528928

840 Kleimenova N. G., Kozyreva O. V., Rozhnoy A. A. and Soloveva M. S. (2004), Variations in the VLF signal parameters on the Australia-Kamchatka radio path during magnetic storms, Geomagn. Aeron. 44, 385-393.

Koga D., Sobral J. H. A., Gonzalez W. D., Arruda D. C. S., Abdu M. A., deCastilho V. M., Mascarenhas M., Gonzalez A. C., Tsurutani B. T., Denardini C. M., and Zamlutti C. J. (2011), Electro-dynamic coupling processes between the magnetosphere and the equatorial ionosphere during a 5-day HILDCAA event, J. Atmos. Solar Terr. Phys., 73, 148-155.

845 Kozyra J. U, G. Crowley, B. A. Emery, X. Fang, G. Maris, M. G. Mlynczak, R. J. Niciejewski, S. E. Palo, L. J. Paxton, C. E. Randall, P.P. Rong, J. M. Russell III, W. Skinner, S. C. Solomon, E. R. Talaat, Q. Wu and J.H. Yee (2006), Response of the Upper/Middle Atmosphere to Coronal Holes and Powerful High-Speed Solar Wind Streams in 2003. Recurrent Magnetic Storms: Corotating Solar Wind Streams. Geophysical Monograph 167. Edited by Bruce Tsurutani, Robert McPherron, Walter Gonzalez, Gang Lu, Jose H. A. Sobral and Natchimuthukonar Gopalswamy. ISBN-13: 978-0-87590-432-0. AGU Books Board, AGU, Washington, DC USA, 319.

850 Kulyamin D.V. and V.P. Dymnikov (2016), Numerical modelling of coupled neutral atmospheric general circulation and ionosphere D region, Russian Journal of Numerical Analysis and Mathematical Modelling, 31, 3, pp. 159-171. doi: https://doi.org/10.1515/rnam-2016-0016

Kumar A. and Kumar S. (2014), Space weather effects on the low latitude D-region ionosphere during solar minimum. Earth, Planets and Space, 66.

Kumar A. and S. Kumar (2020), Ionospheric D region parameters obtained using VLF measurements in the South Pacific region, J. Geophys.
855 Res. Space Phys., 125, e2019JA027536. doi: https://doi.org/10.1029/2019JA027536

Kumar S., A. Kumar, F. Menk, A.K. Maurya, R. Singh and B. Veenadhari (2015), Response of the low-latitude D region ionosphere to extreme space weather event of 14–16 December 2006, J. Geophys. Res. Space Physics, 120, pp. 788–799.

Kutiev I., Ioanna Tsagouri, Loredana Perrone, Dora Pancheva, Plamen Mukhtarov, Andrei Mikhailov, Jan Lastovicka, Norbert Jakowski, Dalia Buresova, Estefania Blanch, Borislav Andonov, David Altadill, Sergio Magdaleno, Mario Parisi and Joan Miquel Torta (2013),
860 Solar activity impact on the Earth's upper atmosphere, Journal of Space Weather and Space Climate, 3.

Lauter E.A. and R.H. Knuth (1967), Precipitation of high energy particles into the upper atmosphere at medium latitudes after magnetic storms, J. Atmos. Solar-Terr. Phys., 29, 4, pp. 411-417. doi: 10.1016/0021-9169(67)90023-2

Lanzagorta (2012), Underwater Communications (Synthesis Lectures on Communications), Morgan & Claypool Publishers, San Rafael, California (USA), 129 p. doi: https://doi.org/10.2200/S00409ED1V01Y201203COM006

865 Lastovicka J. (1989), Solar wind and high energy particle effects in the middle atmosphere, Handb. MAP, 29, 119.

Lastovicka J. (1996), Effects of geomagnetic storms in the lower ionosphere, middle atmosphere and troposphere, J. Atm. Sol. Terr. Phys., 58, 831-843.

Laughlin L.K., N.E. Turner and E.J.J. Mitchell (2008), Geoeffectiveness of CIR and CME Events: Factors Contributing to Their Differences, Southeast. Assoc. Res. Astron., 2, pp. 19-22.

870   Le H., L. Liu, Z. Ren, Y. Chen, H. Zhang and W. Wan (2016), A modeling study of global ionospheric and thermospheric responses to extreme solar flare, J. Geophys. Res. Space Physics, 121, pp. 832– 840. doi:10.1002/2015JA021930

Lincoln, J.V. (1964), The listing of sudden ionospheric disturbances, Planet. Space Sci., 12, 5, pp. 419-434, doi: https://doi.org/10.1016/0032-0633(64)90035-2.

Lodge, O. (1902), Mr. Marconi's Results in Day and Night Wireless Telegraphy, Nature, 66, 1705, p. 222. https://doi.org/10.1038/066222c0

875   Lu G., Cowley S. W. H., Milan S. E., Sibeck D. G., Greenwald R. A., Moretto T. (2002), Solar wind effects on ionospheric convection: a review, J. Atm. Solar-Terr. Phys., 64, 145-157.

Liu S.L. and L.W. Li (2002), Study on Relationship between Southward IMF Events and Geomagnetic Storms, Chinese J. Geophys., 45, 3, pp. 301-310. doi: https://doi.org/10.1002/cjg2.243

Lynn K.J.W. (1978), Some differences in diurnal phase and amplitude variations for VLF signals, J. Atmos. Terr. Phys., 40, 2, pp. 145-150,
880   doi: https://doi.org/10.1016/0021-9169(78)90018-1

Machol, J., M. Snow, D. Woodraska, T. Woods, R. Viereck and O. Coddington (2019) An improved lyman-alpha composite, Earth Space Sci., 6, pp. 2263-2272. https://doi.org/10.1029/2019EA000648

Marconi, G. (1901), Syntonic Wireless Telegraphy, J. Soc. Arts, 49, 2530, pp. 505-520, www.jstor.org/stable/41335571.

Mangla and Yadov (2011) $https://www.electronics-notes.com/articles/antennas-propagation/ionospheric/ionospheric-$
885    $layers-regions-d-e-f1-f2.php$

Mannucci A.J., B.D. Wilson, D.N. Yuan, C.H. Ho, U.J. Lindqwister and T.F. Runge (1998), A global mapping technique for GPS-derived ionospheric total electron content measurements, Radio Sci., 33, 3, pp. 565–582. doi:10.1029/97RS02707

Mannucci A.J., C.O. Ao and W. Williamson (2020), GNSS Radio Occultation, In Position, Navigation, and Timing Technologies in the 21st Century, eds MortonY.T.J., F. Diggelen, J.J. Spilker, B.W. Parkinson, S. Lo and G. Gao), Chapter 33, pp. 971-1013,
890   https://doi.org/10.1002/9781119458449.ch33

Marr, G.V. (1965), The penetration of solar radiation into the atmosphere, Proc. R. Soc. Lond. A, 288, 1415, pp. 531-539. http://doi.org/10.1098/rspa.1965.0239

Maurya A.K., K. Venkatesham, S. Kumar, R. Singh, P. Tiwari and A.K. Singh (2018), Effects of St. Patrick's Day geomagnetic storm of March 2015 and of June 2015 on low-equatorial D region ionosphere. J. Geophys. Res.: Space Phys., 123, pp. 6836-6850. doi:
895   https://doi.org/10.1029/2018JA025536

Mayaud P.N. (1980) Derivation, Meaning, and Use of Geomagnetic Indices, Geophysical Monograph Series, Volume 22, ISBN:9780875900223, DOI:10.1029/GM022

McCormick J.C. and M.B. Morris (2018), D region Ionospheric Imaging Using VLF/LF Broadband Sferics, Forward Modeling, and Tomography, 25th International Lightning Detection Conference and 7th International Lightning Meteorology Conference, 12-15 March 2018,
900   Ft. Lauderdale, FL, Available: Last accessed: 27 Oct 2021.

McIlwain C.E. (1961), Coordinates for mapping the distribution of magnetically trapped particles, J. Geophys. Res., 66, 11, pp. 3681-3691. doi:10.1029/JZ066i011p03681

McPherron R., Weygand J., Tung-Shin Hsu (2008), Response of the Earth's magnetosphere to changes in the solar wind. J. Atm. Solar-Terr. Phys., 70(2), 303-315. DOI: 10.1016/j.jastp.2007.08.040

905   McPherron, R.L. (1979), Magnetospheric substorms, Rev. Geophys., 17, 4, pp. 657–681. doi:10.1029/RG017i004p00657

McRae W. M. and Thomson N. R. (2004), Solar flare induced ionospheric D-region enhancements from VLF phase and amplitude observations, J Atm. Solar-Terres. Phys., 66, 77-87. DOI:10.1016/j.jastp.2003.09.009

McRae W.M. and N.R. Thomson (2000), VLF phase and amplitude: daytime ionospheric parameters, J. Atmos. Sol. Terr. Phys, 62, 7, pp. 609-618, doi: https://doi.org/10.1016/S1364-6826(00)00027-4.

910   Moore, R.K. (1967), Radio communication in the sea, IEEE Spectrum, 4, 11, pp. 42-51. doi: 10.1109/MSPEC.1967.5217169.

Mironova I., M. Sinnhuber, G. Bazilevskaya, M. Clilverd, B. Funke, V. Makhmutov, E. Rozanov, M.L. Santee and T. Sukhodolov (preprint2021), Exceptional middle latitude electron precipitation detected by balloon observations: implications for atmospheric composition, Atmos. Chem. Phys., xx, pp. xx-xx. https://doi.org/10.5194/acp-2021-737

Mitra W. B. (1974), Ionospheric effects of solar flares, D. Reidel Publishing Company, Dordrecht, Holland.

915   Mittal, N., A. Gupta, P.S. Negi and U. Narain (2011), On Some Properties of SEP Effective CMEs, International Scholarly Research Notice, 2011, Article ID 727140, 6 p. doi: https://doi.org/10.5402/2011/727140

Miyoshi Y., S. Kurita, S.-I. Oyama, Y. Ogawa, S. Saito, I. Shinohara, A. Kero, E. Turunen, P. T. Verronen, S. Kasahara, S. Yokota, T. Mitani, T. Takashima, N. Higashio, Y. Kasahara, S. Matsuda, F. Tsuchiya, A. Kumamoto, A. Matsuoka, T. Hori, K. Keika, M. Shoji, M. Teramoto, S. Imajo, C. Jun and S. Nakamura (2021), Penetration of MeV electrons into the mesosphere accompanying pulsating aurorae, Sci. Rep.,

920   11, 13724. doi: https://doi.org/10.1038/s41598-021-92611-3

Moler WF. (1960), VLF propagation effects of a D-region layer produced by cosmic rays, J. Geophys. Res., 65, 5, pp. 1459-1468. doi: 10.1029/JZ065i005p01459

Moral A.C., E.C.K. Eyiguler and Z. Kaymaz (2013), Sudden Ionospheric Disturbances and their detection over Istanbul, 2013 6th International Conference on Recent Advances in Space Technologies (RAST), Istanbul, Turkey, 12 - 14 June 2013, pp. 765-768. doi:

925   10.1109/RAST.2013.6581313

Muraoka Y. (1979), Lower ionospheric disturbances observed in long-distance VLF transmission at middle latitude, J. Atmos. Terr. Phys., 41, pp. 1031-1042, doi: https://doi.org/10.1016/0021-9169(79)90106-5

Naidu P.P., T. Madhavilatha and M.I. Devi (2020), Influence of geomagnetic storms on the mid latitude D and F2 regions, Ann. Geophys., 63, 2, GM214, 13 p. doi: https://doi.org/10.4401/ag-8127

930   Nava B., J. Rodriguez-Zuluaga, K. Alazo-Cuartas, A. Kashcheyev, Y. Migoya-Orue, S.M. Radicella, C. Amory-Mazaudier and R. Fleury (2016), Middle- and low-latitude ionosphere response to 2015-St. Patrick's Day geomagnetic storm, J. Geophys. Res. Space Physics, 121(4), 3421-3438.

Neal J.J., C.J. Rodger and J.C. Green (2013), Empirical determination of solar proton access to the atmosphere: Impact on polar flight paths, Space Weather, 11, 7, pp. 420-433. doi: 10.1002/swe.20066

935   Neal J.J., C.J. Rodger, N.R. Thomson, M.A. Clilverd, T. Raita and T. Ulich (2015), Long-term determination of energetic electron precipitation into the atmosphere from AARDDVARK subionospheric VLF observations, J. Geophys. Res. Space. Phys., 120, 3, pp. 2194-2211. doi: 10.1002/2014JA020689

National Geographic Data Centre, 1996. Ionospheric Digital Database: Worldwide Vertical Incidence Parameters. National Geographic Data Centre, NOAA Boulder, Colorado, USA.

940   Nicolet, M. and A.C. Aikin (1960), The formation of the D region of the ionosphere, J. Geophys. Res., 65, 5, pp. 1469-1483. doi:10.1029/JZ065i005p01469

Nina A., Nico, G., Mitrović, S. T., Čadež, V. M., Milošević, I. R., Radovanović, M., & Popović, L. Č. (2021). Quiet Ionospheric D-Region (QIonDR) Model Based on VLF/LF Observations. Remote Sensing, 13(3), 483.

NOAA SWPC (Retrieved 2012), Solar Particle and Geomagnetic Indices. $swpc.noaa.gov/ftpmenu/indices/old\_indices.html$

945   NOAA SWPC (Retreived 2015), Solar wind speed, proton/particle density and magnetic field components. $ftp : //sohoftp.nascom.nasa.gov/sdb/goes/ace/$

NOAA SWPC (Retreived 2015), Auroral Electrojet (AE) Index. $ftp : //ftp.ngdc.noaa.gov/STP/GEOMAGNETIC_DATA/INDICES/AURO$

NOAA (Retrieved 2016), Geomagnetic Storms, NOAA Space Weather Prediction Center, $http : //www.ngdc.noaa.gov/phenomena/geomagnetic - storms$

950   Nunn D., Clilverd, M. A., Rodger, C. J., & Thomson, N. R. (2004). The impact of PMSE and NLC particles on VLF propagation. In Annales Geophysicae (Vol. 22, No. 5, pp. 1563-1574). Copernicus GmbH.

Nwankwo V. U. J., Chakrabarti S. K. and R. S. Weigel (2015), Effects of plasma drag on low Earth orbiting satellites due to solar forcing induced perturbations and heating, Adv. Space Res., 56, 47-56.

Nwankwo V. U. J., Chakrabarti S. K. and Ogunmodimu O. (2016), Probing geomagnetic storm-driven magnetosphere-ionosphere dynamics
955   in D-region via propagation characteristics of very low frequency radio signals, J. Atmos. Sol-Terres. Phys., 145, 154-169.

Nwankwo, V.U.J. and Chakrabarti, S.K. (2018) Effects of space weather on the ionosphere and LEO satellites' orbital trajectory in equatorial, low and middle latitude. Adv. Space Res., 61(7), 1880-1889, doi:https://doi.org/10.1016/j.asr.2017.12.034.

Nwankwo V.U.J., Chakrabarti S.K., Sasmal S., Denig W. et al. (2020b). Radio aeronomy in Nigeria: First results from very low frequency (VLF) radio waves receiving station at Anchor University, Lagos. 2020 IEEE-ICMCECS, Lagos, Nigeria, pp 1-7, DOI: 10.1109/ICM-
960   CECS47690.2020.247002.

Nwankwo V.U.J., Raulin J-P., Correia E., Denig W., Folarin O., Ogunmodimu O. and De Oliveira R.R. (2021), Investigation of iono-sphere response to geomagnetic storms over the propagation paths of very low frequency radio waves. Submitted to AGU Radio Science, 2021RS0007331.

Ouattara, F., Amory-Mazaudier, C., Fleury, R., Lassudrie Duchesne, P., Vila, P.,Petitdidier, M. (2009), West African equatorial ionospheric
965   parameters climatology based on Ouagadougou ionosonde station data from June 1966 to February 1998. Ann. Geophys. 27, 2503-2514.

Palit S., Basak, T., Mondal, S.K., Pal, S., Chakrabarti, S.K., 2013. Modeling of very low frequency (VLF) radio wave signal profile due to solar flares using the GEANT4 Monte Carlo simulation coupled with ionospheric chemistry. Atmos. Chem. Phys. 13, 9159-9168.

Pavlov, A.V. (2012), Ion Chemistry of the Ionosphere at E- and F-Region Altitudes: A Review, Surv. Geophys. 33, pp. 1133-1172. doi: https://doi.org/10.1007/s10712-012-9189-8

970   Pederick L.H. and M.A. Cervera (2014), Semiempirical Model for Ionospheric Absorption based on the NRLMSISE-00 atmospheric model, Radio Sci., 49, 2, pp. 81-93. doi: 10.1002/2013RS005274

Pedersen A. (1962), Time, height, and latitude distribution of D layers in the subauroral zone and their relation to geomagnetic activity and aurora, J. Geophys. Res., 67, 7, pp. 2685–2694. doi: 10.1029/JZ067i007p02685

Peter W. B., Chevalier M. W., and Inan U. S. (2006), Perturbations of mid-latitude sub-ionospheric VLF signals associated with lower
975   ionospheric disturbances during major geomagnetic storms, J Geophys. Res., 111, AO3301.

Pierce (1969), Sferics, Conference Proceedings, NAS-NRC Atmospheric Exploration by Remote Probes, Vol. 2, NTRS 19720017733, 25 p.

Pierce, J.A. (1955), The Diurnal Carrier-Phase Variation of a 16-Kilocycle Transatlantic Signal, Proc. IRE, 43, 5, pp. 584-588. doi: 10.1109/JRPROC.1955.278102

Poole I. (1999), Radio Waves and the Ionosphere, in QST (Calling All Stations), November 1999, monthly publication of the American
980   Radio Relay League (ARRL), 3 p. Available "$http : //www.arrl.org/qst$" , Last accessed: 20211213

Potemra T.A., A.J. Zmuda, B.W. Shaw and C.R. Have (1970), VLF phase disturbances, HF absorption, and solar protons in the PCA events of 1967, Radio Sci., 5, 8-9, pp. 1137-1145. doi: 10.1029/RS005i008p01137

Porazik P., Johnson, J. R., I. Kaganovich and E. Sanchez (2014), Modification of the loss cone for energetic particles, Geophys. Res. Lett., 41, 22, pp. 8107–8113. doi: 10.1002/2014GL061869

985 Prol F.S., T. Kodikara, M.M. Hoque and C. Borries (2021), Global-scale ionospheric tomography during the March 17, 2015 geomagnetic storm, Space Weather, 19, e2021SW002889, 21 p. doi: https://doi.org/10.1029/2021SW002889

Prolss G. W. (2004), Physics of the Earth's space environment, ISBN: 978-3-540-21426-7, pp. 159-208, Springer Berlin Heidelberg, Germany. doi: $https://doi.org/10.1007/978-3-642-97123-5_4$

Quan, L., B. Cai, X. Hu, Q. Xu and L. Li (2021), Study of ionospheric D region changes during solar flares using MF radar measurements, 990 Adv. Space Res., 67, 2, pp. 715-721. doi: https://doi.org/10.1016/j.asr.2020.10.015

Raghav A., Z. Shaikh, D. Misal, G. Rajan, W. Mishra, S. Kasthurirangan, A. Bhaskar, N. Bijewar, A. Johri and G. Vichare (2020), Exploring the common origins of the Forbush decrease phenomenon caused by the interplanetary counterpart of coronal mass ejections or corotating interaction regions, Phys. Rev. D, 101, 062003. doi: https://doi.org/10.1103/PhysRevD.101.062003

Raulin, J.-P., Pacini, A.A., Kaufmann, P., Correia, E., Martinez, M.A.G. (2010). On the detectability of solar X-ray flares using very low 995 frequency sudden phase anomalies, J Atmo. Solar-Terres. Phys., 68, 1029-1035.

Rawer, K. (1981), Introduction to IRI 1979, in International Reference Ionosphere IRI 97, UAG-82, World Data Center A for Solar-Terrestrial Physics, eds. Lincoln, J.V. and R.O Conkright, pp. 1-6. Available at "$https://www.ngdc.noaa.gov/stp/space-weather/online-publications/stp\_uag/$", Last accessed: 02 December 2021

Rawer, K., D. Bilitza and S. Ramakrishnan, S. (1978), Goals and status of the International Reference Ionosphere, Rev. Geophys., 16, 2, pp. 1000 177–181. doi:10.1029/RG016i002p00177

Reeves G.D. and I.A. Daglis (2016), Geospace Magnetic Storms and the Van Allen Radiation Belts, in "Waves, Particles, and Storms in Geospace : A Complex Interplay", Chapter 3, eds. Balasis, G., I.A. Daglis and I.R. Mann, doi: 10.1093/acprof:oso/9780198705246.003.0004

Reeves G.D., H.E. Spence, M.G. Henderson, S.K. Morley, R.H. Friedel, H.O. Funsten, D.N. Baker, S.G. Kanekal, J.B. Blake, J.F. Fennell, 1005 S.G. Claudepierre, R.M Thorne, D.L. Turner, C.A. Kletzing, W.S. Kurth, B.A. Larsen and J.T. Niehof (2013), Electron acceleration in the heart of the Van Allen radiation belts, Science, 341, 6149, 991-4. doi: 10.1126/science.1237743

Reinisch B. W. and H. Xueqin (1983), Automatic calculation of electron density profiles from digital ionograms: 3. Processing of bottomside ionograms, Radio Sci., 18, 3, pp. 477–492, doi: 10.1029/RS018i003p00477.

Rishbeth H. (1973), Physics and chemistry of the ionosphere, Contemporary Physics, 14, 3, pp. 229-249. doi: 10.1080/00107517308210752

1010 Reinisch B. W. and H. Xueqin (1983), Automatic calculation of electron density profiles from digital ionograms: 3. Processing of bottomside ionograms, Radio Sci., 18, 3, pp. 477–492, doi: 10.1029/RS018i003p00477.

Ries G., (1967), Results Concerning the Sunrise Effect of VLF Signals Propagated Over Long Paths, Radio Sci., 2, 6, pp. 531-538. doi: 10.1002/rds196726531

Ripoll J.-F., M Denton, V. Loridan, O. Santolík, D Malaspina, D.P. Hartley, G.S. Cunningham, G. Reeves, S. Thaller, D.L. Turner, J.F. 1015 Fennell, A.Y. Drozdov, J.S. Cervantes Villa, Y.Y. Shprits, X. Chu, G. Hospodarsky, W.S. Kurth, C.A. Kletzing, J. Wygant, M.G. Henderson and A.Y. Ukhorshiy (2020), How whistler mode hiss waves and the plasmasphere drive the quiet decay of radiation belts electrons following a geomagnetic storm, J. Phys.: Conf. Ser., 1623, paper 012005, 14th Int. Conf. on Numerical Modeling of Space Plasma Flows: ASTRONUM-2019 1-5 July 2019, Paris, France.

Robinson R.M., A. van Eyken and D. Farley (2009), Fiftieth Anniversary of the First Incoherent Scatter Radar Experiment, Eos Trans. AGU, 1020 90, 31, 267-267. doi:10.1029/2009EO310005.

Robinson R.M. and L.J. Zanetti (2021), Auroral energy flux and Joule heating derived from global maps of field-aligned currents, Geophys. Res. Lett., 48, 7, e2020GL091527. doi: https://doi.org/10.1029/2020GL091527

Rogers N. and F. Honary (2014), D-region HF absorption models incorporating real-time riometer measurements, XXXIth URSI General Assembly and Scientific Symposium (URSI GASS), 2014, pp. 1-2, doi: 10.1109/URSIGASS.2014.6929716

Rodger C. J., Hendry, A. T., Clilverd, M. A., Kletzing, C. A., Brundell, J. B., & Reeves, G. D. (2015). High-resolution in situ observations of electron precipitation-causing EMIC waves. Geophysical Research Letters, 42(22), 9633-9641.

Rodger C.J., M.A. Clilverd, N.R. Thomson, R.J. Gamble, A. Seppälä, E. Turunen, N.P. Meredith, M. Parrot, J.-A. Sauvaud and J.-J. Berthelier (2007), Radiation belt electron precipitation into the atmosphere: Recovery from a geomagnetic storm, J. Geophys. Res., 112, A11307, 22 p. doi: 10.1029/2007JA012383

Rodger, C.J., M.A. Clilverd, A. Seppälä, A., N.R. Thomson, R.J. Gamble, M. Parrot, J.-A. Sauvaud and T. Ulich (2010), Radiation belt electron precipitation due to geomagnetic storms: Significance to middle atmosphere ozone chemistry, J. Geophys. Res., 115, A11320, 12 p. doi:10.1029/2010JA015599

Rodger, C.J., M.A. Clilverd, A.J. Kavanagh, C.E.J. Watt, P.T. Verronen and T. Raita (2012), Contrasting the responses of three different ground-based instruments to energetic electron precipitation, Radio Sci., 47, 2, RS2021, 13 p. doi: 10.1029/2011RS004971

Rogers N.C., A. Kero, F. Honary, P.T. Verronen, E.M. Warrington and D.W. Danskin (2016), Improving the twilight model for polar cap absorption nowcasts, Space Weather, 14, 11, pp. 950–972, doi:10.1002/2016SW001527

Rose D.C. and S. Ziauddin (1962), The Polar Cap Absorption Effect, Space Sci. Rev., 1, 1, pp. 115-134. doi: 10.1007/BF00174638

Rostoker G., S.-I. Akasofu, J. Foster, R. Greenwald, Y. Kamide, K. Kawasaki, A. Lui, R. McPherron and C. Russell (1980), Magnetospheric substorms—definition and signatures, J. Geophys. Res., 85, A4, pp. 1663–1668. doi: 10.1029/JA085iA04p01663

Rozhnoi A., M. Solovieva, V. Fedun, P. Gallagher, J. McCauley, M.Y. Boudjada, S. Shelyag and H.U. Eichelberger (2019), Strong influence of solar X-ray flares on low-frequency electromagnetic signals in middle latitudes, Ann. Geophys., 37, 5, pp. 843-850, doi: 10.5194/angeo-37-843-2019.

Russell C.T. (1991), The Magnetosphere, Annual Rev. Earth Planet. Sci., 19, pp. 169-182. doi: https://doi.org/10.1146/annurev.ea.19.050191.001125

Russell C. T., R.L. McPherron and R.K. Burton (1974), On the cause of geomagnetic storms, J. Geophys. Res., 79, 7, pp. 1105-1109. doi:10.1029/JA079i007p01105

Samanes J.E., J. Raulin, E.L. Macotela and W.R. Guevara Day (2015), Estimating the VLF modal interference distance using the South America VLF Network (SAVNET). Radio Sci., 50, 122– 129. doi: 10.1002/2014RS005582.

Samsonov A.A., Y.V. Bogdanova, G.Branduardi-Raymont, D.G. Sibeck and G. Toth (2020), Is the relation between the solar wind dynamic pressure and the magnetopause standoff distance so straightforward?, Geophysical Research Letters, 47, 8, e2019GL086474. https://doi.org/10.1029/2019GL086474

Satori G. (1991), Combined ionospheric effect due to Forbush decreases and magnetospheric high energy particles at mid-latitudes, J. Atmos. Terr. Phys., 53, 3-4, pp. 325-332. doi: https://doi.org/10.1016/0021-9169(91)90116-O

Sasmal S. and Chakrabarti, S. K. (2009). Ionosperic anomaly due to seismic activities–Part 1: Calibration of the VLF signal of VTX 18.2 KHz station from Kolkata and deviation during seismic events. Natural Hazards and Earth System Sciences, 9(4), 1403-1408.

Sastri J.H. (2006), Effect of magnetic storms and substorms on the low- latitude/ equatorial ionosphere, in Solar Influence on the Heliosphere and Earth's Environment: Recent Progress and Prospects, eds. Gopalswamy, N. and A. Bhattacharyya, Proc. ILWS Workshop in Goa,

India: 19-24 February 2006. Available: $https://cdaw.gsfc.nasa.gov/publications/ilws_goa2006/361\_Sastri.pdf$. Last accessed: 18 Jan 2022.

1060   Sauer H.H. and D.C. Wilkinson (2008), Global mapping of ionospheric HF/VHF radio wave absorption due to solar energetic protons, Space Weather, 6, 12, S12002, doi:10.1029/2008SW000399

Sharma A.K. and C. More (2017), Diurnal Variation of VLF Radio Wave Signal Strength at 19.8 and 24 kHz Received at Khatav India (16° 46'N, 75° 53'E), J. Space Sci. Tech., 6, 2, 12 p. doi: https://doi.org/10.37591/.v6i2.2000

Scherliess L. and B.G. Fejer (1997), Storm time dependence of equatorial disturbance dynamo zonal electric fields, J. Geophys. Res.: Space 1065   Phys., 102, A11, pp. 24037–24046. doi:10.1029/97JA02165

Schunk R.W. (1996), Handbook of Ionospheric Models, Report, Aeronomic Models of the Ionosphere, Solar-Terrestrial Energy Program (STEP), Working Group 3.6, 301 p.

Schunk R.W. (1999), Guide to Reference and Standard Ionosphere, ANSI/AIAA G-034-1998, American National Standards Institute, 67 p.

Schunk R. and A. Nagy (2009), Ionospheres: Physics, Plasma Physics, and Chemistry (2nd ed., Cambridge Atmospheric and Space Science 1070   Series), Cambridge University Press., xx p. doi:10.1017/CBO9780511635342

Schunk R.W., L. Scherliess, J.J. Sojka, D.C. Thompson, D.A. Anderson, M. Codrescue, C. Minter, T.J. Fuller-Rowell, R.A. Heelis and B.M Howe (2004), Global Assimilation of Ionospheric Measurements (GAIM), Radio Sci., 39, RS1S0, 11 p. doi: 10.1029/2002RS002794

Scotto C. and A. Settimi (2014), The calculation of ionospheric absorption with modern computers, Adv. Space Res., 54, 8, pp. 1642-1650. doi: https://doi.org/10.1016/j.asr.2014.06.017

1075   Sechrist C.F. (1974), Comparisons of techniques for measurement of D-region electron densities, Radio Sci., 9, 2, pp. 137-149. doi: 10.1029/RS009i002p00137

Seppälä A., Clilverd, M. A., Beharrell, M. J., Rodger, C. J., Verronen, P. T., Andersson, M. E., and Newnham, D. A.(2015), Substorm-induced energetic electron precipitation: Impact on atmospheric chemistry, Geophys. Res. Lett., 42, 19, pp. 8172-8176. doi:10.1002/2015GL065523

1080   Shue J.-H., P. Song, C.T. Russell, J.T. Steinberg, J.K. Chao, G. Zastenker, O.L. Vaisberg, S. Kokubun, H.J. Singer, T.R. Detman and H. Kawano (1998), Magnetopause location under extreme solar wind conditions, J. Geophys. Res. Space Phys., 103, A8, pp. 17691-17700. doi:10.1029/98JA01103

Shue J.-H., J.K. Chao, H.C. Fu, C.T. Russell, P. Song, K.K. Khurana and H.J. Singer (1997), A new functional form to study the solar wind control of the magnetopause size and shape, J. Geophys. Res.: Space Phys., 102, A5, pp. 9497–9511. doi:10.1029/97JA00196

1085   Sica R. J., and R. W. Schunk (1990), Interpreting vertical plasma drift in the mid-latitude ionosphere using ionosonde measurements, J. Atmos. Terr. Phys., 38, 1567-1571.

Silber I., & Price, C. (2017). On the use of VLF narrowband measurements to study the lower ionosphere and the mesosphere-lower thermosphere. Surveys in Geophysics, 38(2), 407-441.

Simoes F., Pfaff R., Berthelier J. and Klenzing (2012), A Review of Low Frequency Electromagnetic Wave Phenomena Related to 1090   Tropospheric-Ionospheric Coupling Mechanisms, Space Sci. Rev., 168, 551-593.

Singh R., U.P. Verma and A.K. Singh (2016), Exploring Middle Atmosphere (D-Region) by Very Low Frequency (VLF) Waves, International Journal of Latest Technology in Engineering, Management & Applied Science (IJLTEMAS), V, VI, pp. 51-55.

Siskind, D.E., K. Zawdie, F. Sassi, D. Drob and M. Friedrich (2017), Global modeling of the low and mid latitude ionospheric D and lower E regions and implications for HF radio wave absorption, Space Weather, 15, pp. 115– 130. doi:10.1002/2016SW001546.

1095   Spence H.E. (1996), The what, where, when, and why of magnetospheric substorm triggers, Eos Trans. AGU, 77, 9, pp. 81–86. doi: 10.1029/96EO00051

Spies K.P. and J.R. Wait (1961), Mode calculations for VLF propagation in the earth-ionosphere waveguide, NBS Technical Note 114, 116 p., Call Number: QC100 .U5753 no.114 1961, Available: https://archive.org/details/modecalculations114spie/mode/2up, Last accessed: 10 Apr 2020.

1100   Spjeldvik W.N. and R.M. Thorne (1975), A simplified D-region model and its application to magnetic storm after-effects, J. Atmos. Terr. Phys., 37, 10, pp. 1313-1325. doi: https://doi.org/10.1016/0021-9169(75)90124-5

Stoke P. H. (1993), Energetic Electron Power Flux Deposition at Sanae (L=4.0) from Riometer Recording, J Geophys. Res., 98, 19111-19116.

Snay R.A. and T. Soler (2008), Continuously Operating Reference Station (CORS): History, Applications, and Future Enhancements, J. Surv. Eng., 134, 4, pp. 95-104. doi: 10.1061/(ASCE)0733-9453(2008)134:4(95)

1105   Stamper R., C. Davis and J. Bradford (2005), RAL Low-Cost Ionosonde System, paper SM21A-0361, AGU Fall Meeting, 05-09 Dec. 2005, San Francisco, CA U.S.A.

Soni S.L., M.L. Yadav, R.S. Gupta and P.L. Verma (2020), Exhaustive Study of Three-Time Periods of Solar Activity Due to Single Active Regions: Sunspot, Flare, CME, and Geo-effective Characteristics, submitted to Solar Stellar Astrophys., tbd. doi: 10.1007/s10509-020-03905-3

1110   Suvorova A.V. and A.V. Dmitriev (2015), Magnetopause inflation under radial IMF: Comparison of models, Earth and Space Science, 2, 4, pp. 107–114. doi: 10.1002/2014EA000084

Sun, K., W. Cui and C. Chen (2021), Review of Underwater Sensing Technologies and Applications, Sensors, 21, 23, 7849, 28 p. doi: https://doi.org/10.3390/s21237849

Takefu, M. (1989), Bragg scattering of radio waves by ionospheric wavelike irregularities, J. Geomag. Geoelect., 41, 8, pp. 647-672.

1115   Tatsuta K., Hobara Y., Pal S. and Balikhin M. (2015), Sub-ionospheric VLF signal anomaly due to geomagnetic storms: a statistical study, Ann. Geophys., 33, 1457-1467.

Taylor W.L. (1960), Daytime Attenuation Rates in the Very Low Frequency Band Using Atmospherics, J. Res. NBS, 64D, 4, pp. 349-355.

Thomson N. R. (1993). Experimental daytime VLF ionospheric parameters. Journal of Atmospheric and Terrestrial Physics, 55(2), 173-184.

Thomson, N.R. and W.M. McRae (2009), Nighttime ionospheric D region: Equatorial and nonequatorial, J. Geophys. Res., 114, A08305, 1120   doi: 10.1029/2008JA014001.

Thomson N.R., M.A. Clilverd and W.M. McRae (2007), Nighttime ionospheric D-region parameters from VLF phase and amplitude, J. Geophys. Res., 112, A07304, doi: 10.1029/2007JA012271.

Thomson N.R. and M.A. Clilverd (2001), Solar flare induced ionospheric D-region enhancements from VLF amplitude observations, J. Atmos. Solar Terr. Phys., 63, 16, pp. 1729–1737, doi: 10.1016/S1364-6826(01)00048-7.

1125   Timocin E. (2022), Swarm satellite observations of the effect of prompt penetration electric fields (PPEFs) on plasma density around noon and midnight side of low latitudes during the 07–08 September 2017 geomagnetic storm, Adv. Space Res., 69, 3, pp. 1335-1343. doi: https://doi.org/10.1016/j.asr.2021.11.027

Tsurutani B. T., Gonzalez W. D., Gonzalez A. L. C., Tang F., Arballo J. K., and Okada M. (1995), Interplanetary origin of geomagnetic activity in the declining phase of the solar cycle, J. Geophys. Res., 100, 21717-21733.

1130   Tsurutani B. T., Gonzalez W. D., Gonzalez A. L. C., Guarnieri F. L., Gopalswamy N., Grande M., Kamide Y., Kasahara Y., Lu G., Mann I., McPherron R. L., Soraas F., and Vasyliunas V. M. (2006), Corotating solar wind streams and recurrent geomagnetic activity: A review. J. Geophys. Res., 111, A07S01, doi:10.1029/2005JA011273.

Tsurutani, B.T., O.P. Verkhoglyadova, A.J. Mannucci, A. Saito, T. Araki, K. Yumoto, T. Tsuda, M.A. Abdu, J.H.A. Sobral, W.D. Gonzalez, H. McCreadie, G.S. Lakhina and V.M. Vasyliūnas (2008), Prompt penetration electric fields (PPEFs) and their ionospheric effects during the great magnetic storm of 30–31 October 2003, J. Geophys. Res., 113, A05311. doi: 10.1029/2007JA012879

Tsurutani B. T., Echer E., Guarnieri F. L. and Gonzalez W. D. (2011), The properties of two solar wind high speed streams and related geomagnetic activity during the declining phase of solar cycle 23, J. Atmos. Solar-Terr. Phys., 73, 164, doi:10.1016/j.jastp.2010.04.003.

Tsurutani B. T., Gonzalez, W. D., Lakhina, G. S., & Alex, S. (2003). The extreme magnetic storm of 1-2 September 1859. Journal of Geophysical Research: Space Physics, 108(A7).

Turunen E., A. Kero, P.T. Verronen, Y. Miyoshi, S.-I. Oyama and S. Saito (2016), Mesospheric ozone destruction by high-energy electron precipitation associated with pulsating aurora, J. Geophys. Res. Atmos., 121, 19, pp. 11852–11861. doi:10.1002/2016JD025015

Turunen E., P.T. Verronen, A. Seppälä, C.J. Rodger, M.A. Clilverd, J. Tamminen, C.-F. Enell, and T. Ulich (2009), Impact of different energies of precipitating particles on NOx generation in the middle and upper atmosphere during geomagnetic storms, J. Atmos. Solar-Terr. Phys., 71, 10–11, pp. 1176-1189. doi: https://doi.org/10.1016/j.jastp.2008.07.005

Turunen E., H. Matveinen, J. Tolvanen and H. Ranta (1996), D-region ion chemistry model, in STEP Handbook of Ionospheric Models, edited by R.W. Schunk, pp. 1 –25, SCOSTEP Secretariat, Boulder, Colo. (reference STEP Handbook)

Turner N.E., E.J. Mitchell, D.J. Knipp and B.A. Emery (2006), Energetics of Magnetic Storms Driven by Corotating Interaction Regions: A Study of Geoeffectiveness. In Recurrent Magnetic Storms: Corotating Solar Wind Streams (eds B. Tsurutani, R. McPherron, G. Lu, J.H.A. Sobral and N. Gopalswamy). https://doi.org/10.1029/167GM11

Turner D.L., Angelopoulos, V., Li, W., Hartinger, M. D., Usanova, M., Mann, I. R., ... & Shprits, Y. (2013). On the storm-time evolution of relativistic electron phase space density in Earth's outer radiation belt. Journal of Geophysical Research: Space Physics, 118(5), 2196-2212.

Tuve M.A. and G. Breit (1925), Note on a radio method of estimating the height of the conducting layer, Terrestrial Magnetism and Atmospheric Electricity, 30, pp. 15-16.

van Allen J.A., G.H. Ludwig, E.C. Ray and C.E. McIlwain (1958), Observation of High Intensity Radiation by Satellites 1958 Alpha and Gamma, Jet Propulsion, September 1958, American Rocket Society, Inc., 5 p. doi: https://doi.org/10.2514/8.7396

Verbanac G., B. Vršnak, S. Živković, T. Hojsak, A.M. Veronig and M. Temmer (2011), Solar wind high-speed streams and related geomagnetic activity in the declining phase of solar cycle 23, Astron. Astrophys., 533, A49, 6 p. doi: https://doi.org/10.1051/0004-6361/201116615

Verkhoglyadova O. P., Tsurutani B. T., Mannucci A. J., Mlynczak M. G., Hunt L. A., and Runge T. (2013), Variability of ionospheric TEC during solar and geomagnetic minima (2008 and 2009): external high speed stream drivers, Ann. Geophys., 31, 263-276, doi:10.5194/angeo-31-263-2013.

Verronen P.T., M.E. Andersson, D.R. Marsh, T. Kovacs and J.M.C. Plane (2016), WACCM-D—Whole Atmosphere Community Climate Model with D-region ion chemistry, J. Adv. Model. Earth Syst., 8, 2, pp. 954– 975. doi: 10.1002/2015MS000592

Verronen P.T., A. Seppala, M.A. Clilverd, C.J. Rodger, E. Kyrola, C.-F. Enell, T. Ulich and E. Turunen (2005), Diurnal variation of ozone depletion during the October–November 2003 solar proton events, J. Geophys. Res.: Space Phys., 110, A09, A09S32. doi: 10.1029/2004JA010932

Veronig A., M. Temmer, A. Hanslmeier, W. Itruba and M. Messerotti (2002), Temporal aspects and frequency distributions of solar soft X-ray flares, Astron. Astrophys., 382, 3, pp. 1070-1080. https://doi.org/10.1051/0004-6361:20011694

1170   Voss H.D., M. Walt, W.L. Imhof, J. Mobilia and U.S. Inan (1998), Satellite observations of lightning-induced electron precipitation, J. Geophys. Res., 103, A6, pp. 11725–11744. doi:10.1029/97JA02878

Wait J. R. (1959), Diurnal change of ionospheric heights deduced from phase velocity measurements at VLF, Proc. IRE, 47, 998.

Wait J.R. (1960), Terrestrial Propagation of Very-Low-Frequency Radio Waves, J. Res. Nat Bureau Standards, 64D, 2, pp. 153-204. doi: 10.6028/JRES.064D.022.

1175   Wait J.R. (1961), A New Approach to the Mode Theory of VLF Propagation, J. Res. NBS: D. Radio Propagation, 65D, 1, pp. 37-46. doi: 10.6028/JRES.065D.007.

Wait J.R. (1963), A Note on Diurnal Phase Changes of Very-Low-Frequency Waves for Long Paths, J. Geophys. Res., 68, pp. 338-340. doi: 10.1029/JZ068i001p00338.

Wait J.R. (1964), Two-Dimensional Treatment of Mode Theory of the Propagation of VLF Radio Waves, J. Res. NBS, 68D, 1, pp. 81-93.

1180   doi: 10.6028/jres.068d.019.

Wait J.R. (1968), Mode conversion and refraction effects in the Earth-ionosphere waveguide for VLF radio waves, J. Geophys. Res., 73, 11, pp. 3537-3548. doi: 10.1029/JA073i011p03537.

Wait J.R. (1970), Electromagnetic waves in stratified media, ISBN 978-0-08-006636-3, Pergamon Press, Oxford, 609 p. doi: https://doi.org/10.1016/C2013-0-05239-5.

1185   Wait J. R. and Spies K. P. (1964), Characteristics of the Earth-ionosphere wave-guide for VLF radio waves, NBS Tech. Note 300

Walker D. (1965), Phase steps and amplitude fading of VLF signals at dawn and dusk, Radio Sci., 68D, 11, pp. 1435-1443. doi: 10.6028/JRES.069D.155

Waheed-uz-Zaman and M.A.K. Yousufzai (2011), Design and Construction of Very Low Frequency Antenna, J. Basic Applied Sci., 7, 2, pp. 141-145.

1190   WDCG (Retrieved 2014), Geomagnetic Equatorial Dst index, World Data Centre for Geomagnetism, $http://wdc.kugi.kyoto-u.ac.jp/dstdir/index.html$

Wei Y., Hong M., Wan W., Du A., Lei J., Zhao B., Wang W., Ren Z., and Yue X. (2008), Unusually long lasting multiple penetration of interplanetary electric field to equatorial ionosphere under oscillating IMF Bz, Geophys. Res. Lett., 35, L02102, doi:10.1029/2007GL032305.

Weigel R. S. (2010), Solar wind density influence on geomagnetic storm intensity, J. Geophys. Res., 115, A09201,

1195   doi:10.1029/2009JA015062.

Weigel R. S., Baker D. N., Rigler E. J., and Vassiliadis D. (2004), Predictability of large geomagnetic disturbances based on solar wind conditions, IEEE Trans. Plas. Sci., 32, 1506-1510.

Wiltberger M., R.E. Lopez and L.G. Lyon (2003), Magnetopause erosion: A global view from MHD simulation, J. Geophys. Res., 108, A6, 1235, 9 p., doi:10.1029/2002JA009564

1200   Wu C.C., K. Liou, R.P. Lepping, L. Hutting, S. Plunkett, R.A. Howard and D. Socker (2016), The first super geomagnetic storm of solar cycle 24: "The St. Patrick's day event (17 March 2015)", Earth Planet Space, 68, 151, 12p. https://doi.org/10.1186/s40623-016-0525-y

Yokoyama E. and I. Tanimura (1933), Some Long-Distance Transmission Phenomena of Low-Frequency Waves, Radio Eng. Proc. Inst. (Proc. IRE), 21, 2, pp. 263-270. doi: 10.1109/JRPROC.1933.227600.

Youssef, M. (2012) On the relation between the CMEs and the solar flares, NRIAG Journal of Astronomy and Geophysics, 1, 2, pp. 172-178,

1205   doi: 10.1016/j.nrjag.2012.12.014

Yue X., W.S. Schreiner, N. Pedatella, R.A. Anthes, A.J. Mannucci, P.R. Straus and J.-Y. Liu, (2014), Space Weather Observations by GNSS Radio Occultation: From FORMOSAT-3/COSMIC to FORMOSAT-7/COSMIC-2, Space Weather, 12, 11, p. 616–621, doi: 10.1002/2014SW001133

Zawedde A.E., H. Nesse Tyssøy, J. Stadsnes and M.I. Sandanger (2018), The impact of energetic particle precipitation on mesospheric OH – Variability of the sources and the background atmosphere, J. Geophys. Res.: Space Phys., 123, 7, pp. 5764-5789. doi: https://doi.org/10.1029/2017JA025038

Zesta E. and D.M. Oliveira (2019), Thermospheric heating and cooling times during geomagnetic storms, including extreme events, Geophys. Res. Lett., 46, 22, pp. 12739–12746. doi: https://doi.org/10.1029/2019GL085120

1210